Material Matters™

Vol. 3, No. 1

ALDRICH Chemistry

3-D Nano and Micro Structures

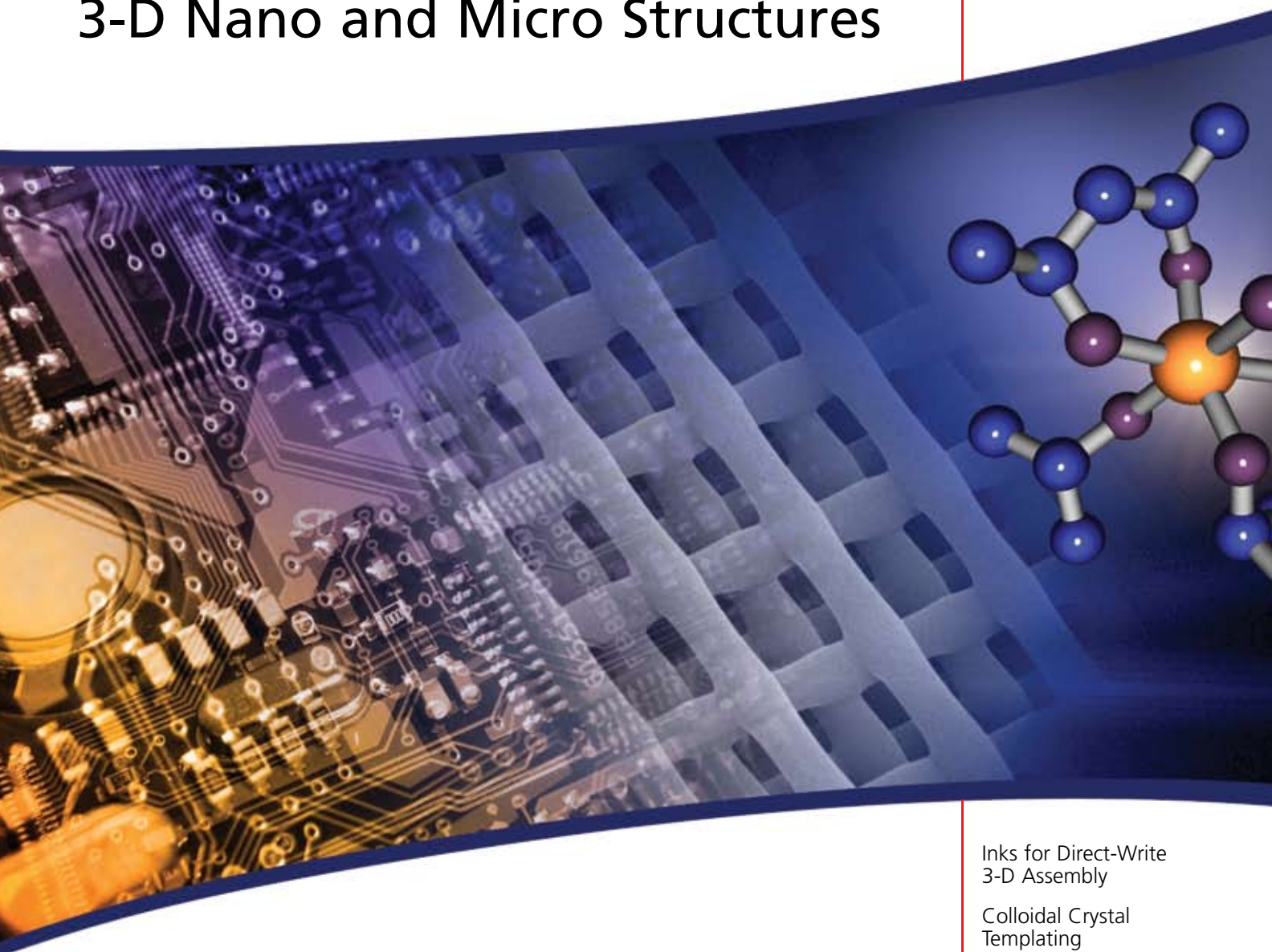

Small Structures Inspiring Big Technologies

Inks for Direct-Write 3-D Assembly

Colloidal Crystal Templating

Electrospinning

Quantum Dots: Nanoscale Synthesis and Micron-Scale Applications

Introduction

Welcome to the first 2008 issue of *Material Matters*™, focusing on 3-dimensional (3D) micro- and nanostructures. New techniques to create materials ordered at micro- and nanoscale drive scientific and technological advances in many areas of science and engineering. For example, 3D-patterned metal oxides could enable construction of micro-fuel cells and high-capacity batteries smaller and more energy efficient compared to presently available devices. Ordered porous materials with exceedingly large surface areas are good candidates for highly efficient catalysts and sensors. New methods for periodic patterning of semiconductor materials are fundamental to next-generation electronics, while individual nanoscale semiconductor structures, known as quantum dots (QDs), have remarkable optical properties for optoelectronics and imaging applications. And biomedical engineers are using tailored nanofibers and patterned polymeric structures to develop tissue-engineering scaffolds, drug-delivery devices and microfluidic networks.

The broad diversity of potentially relevant material types and architectures underscores the need for new approaches to make 3D micro- and nanostructures. In this issue, Professor Jennifer Lewis (University of Illinois at Urbana-Champaign) describes direct-write printing of 3D periodic arrays. This work depends on formulation of suitable inks, many of which can be prepared using particles and polyelectrolytes available from Sigma-Aldrich®. Researchers from the University of Minnesota write about colloidal templating of 3D-ordered materials. A sol-gel precursor selection table and an application note on making colloidal templates accompany the article. Dr. Jingwei Xie and Professor Younan Xia (Washington University, St. Louis) describe electrospinning — a versatile technique for preparation of precise nanoscale polymer and ceramic fibers. The article is accompanied by a selection of polymer products that can be electrospun into nanofibers. Finally, researchers from Nanoco Technologies, Ltd. (Manchester, UK), describe methods for reproducible high-volume synthesis of colloidal QDs. Through the partnership between Nanoco and Sigma-Aldrich, these high-quality QD nanostructures are now available to help you work toward new structured materials and applications.

We hope that the articles and Sigma-Aldrich products featured in this issue will help you in your work. Please contact Aldrich Materials Science at ***matsci@sial.com*** if you need a material that you cannot find in this issue or in our catalog.

Ilya Koltover, Ph.D.
Materials Science
Sigma-Aldrich Corporation

About Our Cover

Photonic band gap (PBG) materials are an exciting application of 3D nanostructures. Periodic PBGs are designed to affect motion of photons in a similar way that periodic semiconductor crystals affect electrons, allowing only propagation of light with certain wavelengths or along defined directions. Potential PBG applications include omni-directional mirrors and low-loss-waveguides that will become building blocks of future all-optical integrated circuits. PBGs are made from dielectric or metallo-dielectric nanostructures, such as the titanium dioxide lattice shown on the cover of this issue. This lattice was made using a direct-write technique developed by Prof. Jennifer Lewis (see article on p. 4) and using titanium diisopropoxide bis(acetylacetonate) precursor (molecule on the right-side of the cover) purchased from Sigma-Aldrich.

Material Matters™
Vol. 3 No. 1

Aldrich Chemical Co., Inc.
Sigma-Aldrich Corporation
6000 N. Teutonia Ave.
Milwaukee, WI 53209, USA

To Place Orders

Telephone	800-325-3010 (USA)
FAX	800-325-5052 (USA)

Customer & Technical Services

Customer Inquiries	800-325-3010
Technical Service	800-231-8327
SAFC®	800-244-1173
Custom Synthesis	800-244-1173
Flavors & Fragrances	800-227-4563
International	414-438-3850
24-Hour Emergency	414-438-3850
Web site	sigma-aldrich.com
Email	aldrich@sial.com

Subscriptions

To request your **FREE** subscription to *Material Matters*, please contact us by:

Phone: **800-325-3010** (USA)

Mail: **Attn: Marketing Communications**
Aldrich Chemical Co., Inc.
Sigma-Aldrich Corporation
P.O. Box 355
Milwaukee, WI 53201-9358

Email: **sams-usa@sial.com**

International customers, please contact your local Sigma-Aldrich office. For worldwide contact information, please see back cover.

Material Matters is also available in PDF format on the Internet at **sigma-aldrich.com/matsci**.

Aldrich brand products are sold through Sigma-Aldrich, Inc. Sigma-Aldrich, Inc. warrants that its products conform to the information contained in this and other Sigma-Aldrich publications. Purchaser must determine the suitability of the product for its particular use. See reverse side of invoice or packing slip for additional terms and conditions of sale.

All prices are subject to change without notice.

Material Matters (ISSN 1933–9631) is a publication of Aldrich Chemical Co., Inc. Aldrich is a member of the Sigma-Aldrich Group.

© 2008 Sigma-Aldrich Co.

"Your Materials Matter."

Joe Porwoll, President
Aldrich Chemical Co., Inc.

Do you have a compound that you wish Sigma-Aldrich® could list to help materials research? If it is needed to accelerate your research, it matters—please send your suggestion to ***matsci@sial.com*** *and we will be happy to give it careful consideration.*

1,3,5-Tris(4-carboxyphenyl)benzene: NEW Building Block for Metal Organic Frameworks

Dr. Channing Ahn of the California Institute of Technology kindly suggested that we make 1,3,5-tris(4-carboxyphenyl)-benzene (BTB) — a building block for Metal Organic Frameworks (MOFs). MOFs are a class of 3D-microporous materials with potential applications in adsorption and separation technologies.[1–3] BTB can be used as a linker to make MOFs with very high surface area, such as MOF-177: a hydrogen absorbing material with an extremely high storage capacity of 7.5% at 77K.[3]

References:

(1) Kubas, G. J., *Chem. Rev.* **2007**, 107, 4152
(2) Walton, K. S.; Millward, A. R.; Dubbeldam, D.; Frost, H.; Low, J. J.; Yaghi, O. M.; Snurr, R. Q. *J. Am. Chem. Soc.*, **2008**, 130, 406.
(3) Wong-Foy A. G., Matzger A.J., Yaghi O. M. *J. Am. Chem. Soc.* **2006**, 128, 3494.

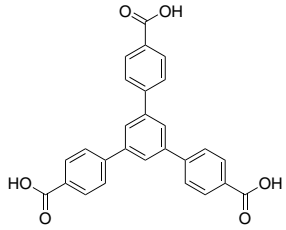

1,3,5-Tris(4-carboxyphenyl)benzene, (BTB)	
686859-1G	1 g

Materials and Synthetic Tools for 3D-Structures Featured in This Issue

Materials Category	Content	Page
Micro-and Nanoscale Powders	Ceramic and metal particulate materials for syntehsis of 3D micro- and nanostructures.	7
Polyelectrolytes	Anionic and cationic polymers with various molecular weights and charged functional groups.	8
Sol-Gel Precursors	Alkoxide, acetylacetonate and acetate precursors for structured metal oxides.	14
Oxalate Salts	Metal oxalate salts for thermal synthesis of structured metal oxides, carbonates and metals.	16
Mesoporous Materials	Silica and alumina mesoporous molecular sieves.	18
Structure Directing Amphiphiles	Surfactants and block copolymers for templated synthesis of ordered structures.	18
Polymers for Electrospinning	Synthetic, biodegradable and natural polymers suitable for electrospinning of nanofibers.	22
Quantum Dots	New core-shell luminescent semiconductor nanocrystals.	27

Novel Inks for Direct-Write Assembly of 3-D Periodic Structures

Prof. Jennifer A. Lewis

Materials Science and Engineering Department
Frederick Seitz Materials Research Laboratory
University of Illinois at Urbana-Champaign

Introduction

New methods for materials fabrication at the micro- and nanoscale will drive scientific and technological advances in areas of materials science, chemistry, physics, and biology. The broad diversity of potentially relevant materials, length scales, and architectures underscores the need for flexible patterning approaches. One important example is the fabrication of 3D periodic structures composed of colloidal,[1] polymeric,[2–4] or semiconductor[5] materials. These structures may find potential application as sensors,[6] microfluidic networks,[7] self-healing materials,[8] photonic band gap materials,[9] and tissue engineering scaffolds.[10] Several strategies have recently emerged for precisely assembling 3D periodic arrays,[1–5] including colloidal epitaxy,[1] litho-[5] and holographic,[3] and direct-write techniques.[2–4] Of these, only the latter approach offers the materials flexibility, low cost, and ability to construct complex 3D structures required for advances across multidisciplinary boundaries.

This article focuses on our recent efforts to design novel inks for direct-write assembly. Through careful control of ink composition, rheological behavior, and printing parameters, 3D structures that consist of continuous solids, high aspect ratio (e.g., parallel walls) or spanning features can be constructed. Of these, 3-D periodic structures offer the greatest challenge for designing inks, because they contain self-supporting features that must span gaps in the underlying layer(s). Below we first describe the direct-write assembly process. We then introduce several ink designs, including concentrated colloidal and nanoparticle,[10–14] polyelectrolyte,[4–15] and sol-gel[16] inks, that enable the direct-write assembly of 3D periodic architectures of diverse functionality with features ranging from tens of microns to submicron in size. Finally, we highlight the opportunities and challenges associated this approach.

Direct-Write Assembly

The term "direct-write assembly" describes fabrication methods that employ a computer-controlled translation stage, which moves a pattern-generating device, i.e., ink deposition nozzle, to create materials with controlled architecture and composition.[17] Unlike ink-jet printing, our approach relies on extruding a continuous ink filament that is deposited in a layer-by-layer build sequence to generate the desired component of interest. The ink is delivered either under constant displacement or pressure mode through a single or multi-nozzle array. The filament diameter is determined by the nozzle diameter, ink rheology, and deposition speed. The component dimensions, minimum feature size, and build times are dictated in part by the lateral (*x*-*y*) and vertical (*z*) translation distances, resolution, and speed. We have recently implemented two 3-axis, motion-controlled stages in our laboratory, as shown in **Figure 1**. They range from the highest precision stage, which is mounted on an inverted fluorescence microscope and has maximum *x*-*y*-*z* travel distances of 300 µm with nanometer resolution and travel speeds of ~ 1 mm/sec, to a larger area stage, in which the maximum *x*-*y* travel distances exceed several centimeters with a resolution of a tens of nanometers and travel speeds of up to 30 mm/s. These vastly different capabilities allow us to pursue applications that range from photonic crystals to self-healing composites.

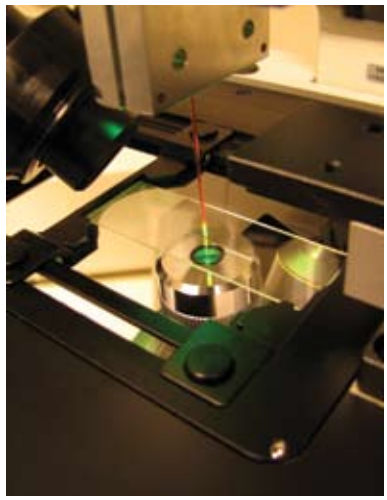

(a)

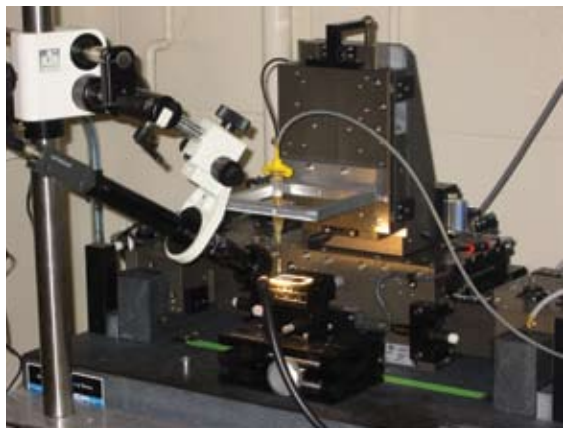

(b)

Figure 1. Photographs of 3-axis, motion-controlled stages utilized in direct-write assembly: (a) high precision stage (*x*-*y*-*z* translation distance = 300x300x300 µm^3, resolution ~ 5 nm, and maximum speed ~ 1 mm/s) and (b) larger-area stage (*x*-*y*-*z* translation distance = 10x10x4 cm^3, resolution ~ 50 nm, and maximum speed = 30 mm/s)..

TO ORDER: Contact your local Sigma-Aldrich office (see back cover),
or visit sigma-aldrich.com/matsci.

Novel Ink Designs

(a) Colloidal and Nanoparticle Inks

Colloidal gels are excellent candidate materials for direct ink writing of complex 3D structures, because their viscoelastic properties can be tailored over many orders of magnitude to facilitate flow through nozzles and produce patterned filaments that maintain their shape, even as they span gaps in the underlying layers of the printed structure.[12] We designed these inks with two important criteria in mind. First, they must exhibit a well-controlled viscoelastic response, so they flow through the deposition nozzle and then "set" immediately to facilitate shape retention of the deposited features even as they spans gaps in the underlying layer(s). Second, they must contain a high colloid volume fraction to minimize drying-induced shrinkage after assembly is complete, so the particle network is able to resist compressive stresses arising from capillary tension. These criteria required careful control of colloidal forces to first generate a highly concentrated, stable dispersion followed by inducing a system change (e.g., ΔpH, ionic strength, or solvent quality) that promotes a fluid-to-gel transition.

Colloidal gels consist of a percolating network of attractive particles capable of transmitting stress above a critical volume fraction, ϕ_{gel}. When stressed beyond their yield point (t_y), they exhibit shear thinning flow behavior due to the attrition of particle-particle bonds within the gel. As the inks flow through the deposition nozzle, they experience a radially varying shear stress. The core of the ink filament remains unyielded and experiences plug-like flow, whereas the outer region of the ink filament exhibits yielding and therefore liquid-like flow.[12] Hence, the ink exits the nozzle as a continuous, rod-like filament with a rigid (gel) core-fluid shell architecture, which simultaneously promotes its shape retention and allows it to fuse with previously patterned features at their contact points. Upon deposition, the fluid shell quickly gels as the attractive particle bonds reform.[12]

We first demonstrated this ink design using a model system consisting of negatively charged, silica microspheres coated with a cationic polyelectrotrolyte, poly(ethylenimine) (PEI) suspended in deionized water.[13] Concentrated silica suspensions (ϕ = 0.46) exhibited a fluid-to-gel transition as their pH was adjusted to a value near their point-of-zero charge. A dramatic rise in elastic properties accompanied this phase transition. Both the shear yield stress and elastic modulus increased by orders of magnitude, because of strengthened interparticle attractions near this pH. Using this ink, 3-D periodic structures were assembled (see **Figure 2**).

This ink design can be readily extended to any type of colloidal material provided their interparticle forces can be controlled to produce the desired solids concentration and rheological properties. In addition to changing pH, the requisite ink rheology may be achieved through the addition of salt, oppositely charged polyelectrolyte species, or other coagulants. These strategies have been employed to produce inks from a broad array of colloidal materials, including silica,[13] lead zirconate titanate,[12] barium titanate,[14] alumina,[18] hydroxyapatite (**04238**),[10] polymer latices,[19] and most recently, metallic nanoparticles. Further reductions in feature size are possible by designing nanoparticle inks, in which the maximum particle diameter is less than 100 nm (see Figure 2). The commercial availability of high quality inorganic, polymeric, and metallic nanoparticles, with precise control over particle composition, shape, size, and size distribution, is highly desirable.

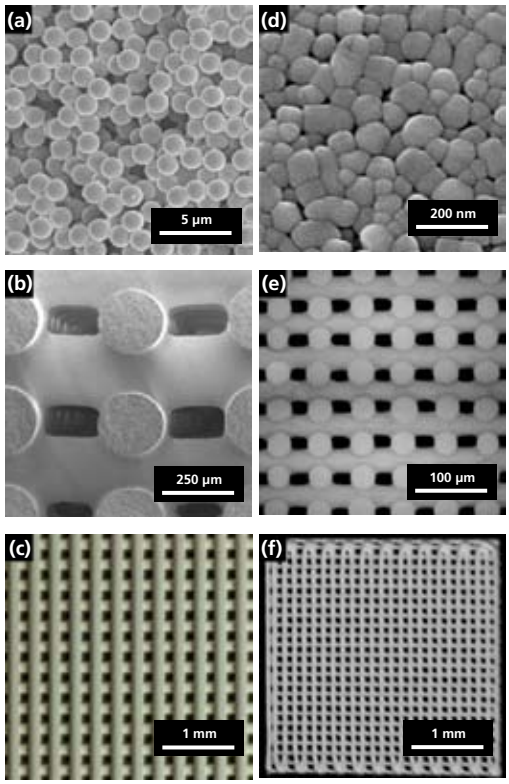

Figure 2. Left column images show (a) SEM micrograph of the model colloidal ink used to print the 3-D periodic lattice (10 layers, 500 µm in-plane pitch, 250 µm rod diameter), shown in both (b) cross-sectional and (c) top views. Right column images show (d) SEM micrograph of a nanoparticle ink used to print the 3-D periodic lattice (16 layers, 200 µm in-plane pitch, 100 µm rod diameter), shown in both (e) cross-sectional and (f) top views. [(a)-(c) from Ref. 13; (d)-(f) from Ref. 14]

(b) Polyelectolyte Inks

It has been a grand challenge to design concentrated inks suitable for direct writing at the microscale. Colloidal inks either experience jamming (or clogging) in the deposition nozzle or require exceedingly large pressures to induce ink flow. To overcome these limitations, we drew inspiration from nature to develop concentrated polyelectrolyte complexes that mimic spider silk in a simplistic way.

This ink design utilizes polyelectrolyte complexes composed of non-stoichiometric mixtures of polyanions and polycations.[4] We first explored mixtures of poly(acrylic acid), PAA and poly(ethyleneimine),PEI that were nominally 40 wt.% polyelectrolyte in an aqueous solution. By regulating the ratio of anionic (COONa) to cationic (NH_x) groups and combining these species under solution conditions that promote polyelectrolyte exchange reactions,[15] we produced homogeneous fluids over a broad compositional range that possessed the requisite viscosities needed for flow through micro-capillary nozzles of varying diameter.

The concentrated polyelectrolyte inks rapidly coagulate to yield self-supporting filaments (or rods) upon deposition into an alcohol/water coagulation reservoir. The exact coagulation mechanism, driven by electrostatics in a water-rich or solvent quality effects in an alcohol-rich reservoir, as well as the magnitude of ink elasticity depend strongly on the alcohol/water ratio. By carefully tuning this parameter, the deposited

ALDRICH Chemistry

ink filament is elastic enough to promote shape retention, while maintaining sufficient flexibility for continuous flow and adherence to the substrate and underlying patterned layers. 3-D micro-periodic scaffolds are created by depositing the PAA-PEI ink into an alcohol-rich reservoir (see Fig. 3). Such structures may find potential application as sophisticated scaffolds that guide the electrostatic layer-by-layer assembly of materials,[4] direct cell-scaffold interactions, or interact with other environmental stimuli, or as templates for biomimetic,[20] photonic, microfluidic,[7] or low-cost MEMs devices.[21] This ink design can be readily extended other polyelectrolyte mixtures,[4,20] including those based on biologically, electrically, or optically active species. For example, it should be relatively straightforward to extend our approach to patterning biological materials, such as silk and polypeptides.

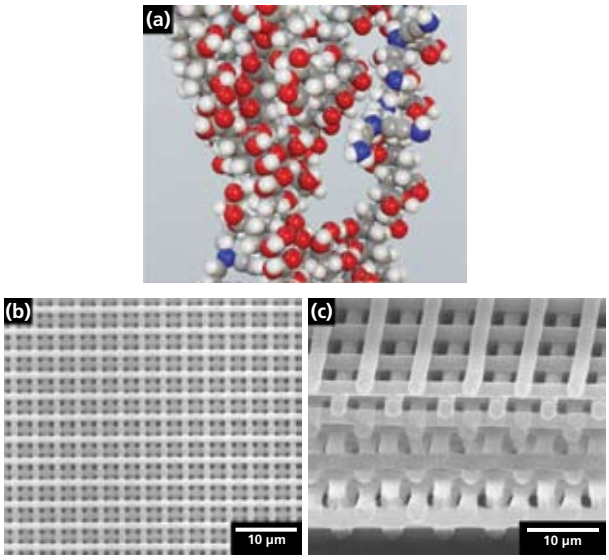

Figure 3. (a) Schematic illustration of the polyelectrolyte ink. (b) SEM image of 3-D micro-periodic lattice (16 layers, 4 µm in-plane pitch, 1 µm rod diameter) assembled by direct ink writing (top view), (c) focused ion beam milled, cross-section showing the excellent alignment between printed layers. [from Ref. 21]

(c) Sol-Gel Inks

The ability to pattern oxide structures at the microscale in both planar and three-dimensional forms is important for a broad range of emerging applications, including sensors, micro-fuel cells and batteries, photocatalysts, solar arrays, and photonic band gap (PBG) materials. By designing sol-gel inks based on organometallic precursors, we have recently demonstrated direct ink writing of micro-periodic oxide structures (see Figure 2d).[16]

Our ink design incorporates a sol-gel precursor solution based on a chelated titanium alkoxide, titanium diisopropoxide bisacetylacetonate (TIA, **325252**).[16] An organic polymer, poly(vinyl pyrrolidone) (PVP, e.g. **234257**), is also included to mitigate stresses that occur during drying and calcination of the as-patterned structures. Unlike the polyelectrolyte inks described above, these sol-gel inks can be patterned directly in air. Using DIW, we created 3D micro-periodic structures composed of parallel arrays of orthogonally stacked rods. To convert these structures to the desired oxide phase, in this case TiO_2, they are calcined at elevated temperatures (> 450 °C). Both the anatase and rutile phases can be generated depending on the precise heat treatment conditions. This sol-gel ink design and patterning approach can be readily extended to other organometallic precursors. For example, by simply varying the organometallic precursors used, we have formulated inks for microscale patterning of electrically (e.g., doped-TiO_2), transparent (e.g., indium tin oxide), and ionically (e.g., doped-zirconium oxide) conducting oxides (Table 1). The broad palette of precursor materials available enables a myriad of potential applications to be pursued.

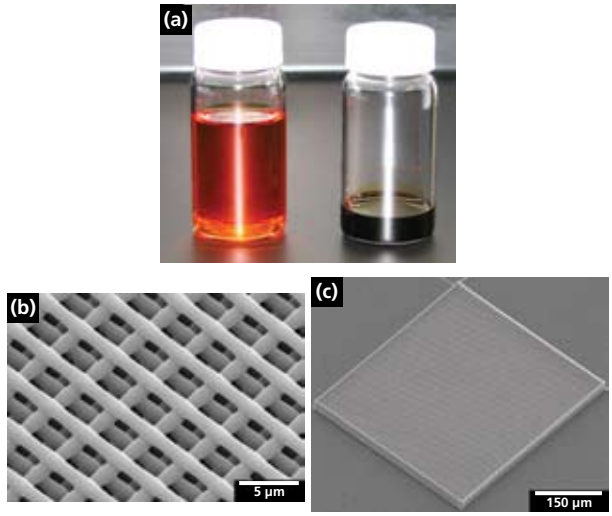

Figure 4. (a) Photographs of the precursor solution (left) and concentrated sol-gel ink after evaporation (right) used to print the 3-D micro-periodic lattice (24 layers, 4 µm in-plane pitch, 1 µm rod diameter), (b) SEM micrograph of top surface (high magnification view) and (c) SEM micrograph of entire lattice. [from Ref. 16]

Opportunities and Challenges

Direct ink writing offers the ability to rapidly pattern functional materials in complex 3D architectures from a diverse array of materials. Using the ink designs highlighted above, the current minimum feature sizes range from approximately 200 µm for colloidal inks to 250 nm for sol-gel inks at characteristic printing speeds of 1–10 mm/s. However, the continual drive towards patterning materials at even finer length scales and faster printing speeds gives rise to many opportunities and challenges. Future advances will require new ink chemistries, better characterization and modeling of ink dynamics during deposition, and enhanced robotic, control, and ink delivery systems to allow three-dimensional writing with greater spatial and composition control. Specific chemistries of interest include semiconducting and metallic nanoparticles as well as novel hydrogel and sol-gel precursors that can be readily formulated with the above considerations in mind.

Acknowledgments

The author gratefully acknowledges the generous support for our work by U.S. Department of Energy through the Frederick Seitz Materials Research Laboratory (Grant# DEFG02-91ER45439), the Army Research Office through the MURI program (Grant# DAAD19-03-1-0227), the National Science Foundation (Grant# 00-99360) and the Air Force Office of Scientific Research through both the MURI (Grant# F49550-05-1-0346) and the DURIP program (Grant# FA9550-06-1-0321). This work has benefited from the valuable contributions of J. Cesarano, J. Smay, G. Gratson, M. Xu, R. Shepherd, R. Rao, E. Duoss, D. Lorang, S. White, N. Sottos, D. Therriault, K. Toohey, C. Hansen, W. Wu, and J. Bukowski.

TO ORDER: Contact your local Sigma-Aldrich office (see back cover), or visit sigma-aldrich.com/matsci.

References:

(1) van Blaaderen, A.; Ruel, R.; Wiltzius, P. *Nature* **1997**, *385*, 321. (2) Cumpston, G.H.; Ananthavel, S.P.; Barlow, S.; Dyer, D.L.; Ehrlich, J.E.; Erskine, L.L.; Heikal, A.A.; Kuebler, S.M.; Lee, I.Y.S.; McCord-Maughon, D.; Qin, J.; Rockel, H.; Rumi, M.; Wu, X.-L.; Marder, S.R.; Perry, J.W. *Nature* **1999**, 398, 51. (3) Campbell, M.; Sharp, D.N.; Harrison, M.T.; Denning, R.G.; Turberfield, A.J. *Nature* **2000**, *404*, 53. (4) Gratson, G.M.; Xu, M.; Lewis, J.A. *Nature* **2004**, *428*, 386. (5) Lin, S.Y.; Fleming, J.G.; Hetherington, D.L.; Smith,B.K.; Biswas, R.; Ho, K.M.; Sigalas, M.M.; Zubrzycki, W.; Kurtz, S.R.; Bur, J. *Nature* **1998**, *394*, 251. (6) Lee, Y.L.; Braun, P.V. *Adv. Mater.* **2003**, *15*, 563. (7) Therriault, D.; White, S.R.; Lewis, J.A. *Nat. Mater.* **2003**, *2*, 265. (8) Toohey, K.S.; Sottos, N.R.; Lewis, J.A.; Moore, J.S.; White, S.R. *Nature Mater.* **2007**, *6*, 581. (9) Joannopoulos, J.D.; Villeneuve, P.R.; Fan, S.H. *Nature* **1997**, *386*, 143. (10) Michna, S.; Wu, W.; Lewis, J.A. *Biomaterials* **2005**, *26*, 5632. (11) Cesarano, J.; Calvert, P. U.S. Patent 6 027 326, **2000**. (12) Smay, J.E.; Cesarano, J.; Lewis, J.A. *Langmuir* **2002**, *18*, 5429. (13) Smay, J.E.; Gratson, G.M.; Shepherd, R.F.; Cesarano, J.; Lewis, J.A. *Adv. Mater.* **2002**, *14*, 1279. (14) Li, Q.; Lewis, J.A. *Adv. Mater.* **2003**, *15*, 1639. (15) Gratson, G.M.; Lewis, J.A. *Langmuir* **2005**, *21*, 457. (16) Duoss, E.B.; Twardowski, M.; Lewis, J.A. *Adv. Mater.* **2007**, *19*, 3485. (17) Lewis, J.A.; Gratson, G.M. *Materials Today* **2004**, *7*, 32. (18) Rao, R.; Morales, A.; Kracik, K.; Lewis, J.A. *Adv. Mater.* **2005**, *17*, 289. (19) Xie, B.; Parkhill, R.L.; Warren, W.L.; Smay, J.E. *Adv. Funct. Mater.* **2006**, *16*, 1685. (20) Xu, M.; Gratson, G.M.; Duoss, E.; Shepherd, R.F.; Lewis, J.A. *Soft Matter* **2006**, *2*, 205. (21) Gratson, G.; Garcia-Santa Maria, F.; Braun, P.V.; Lewis, J.A. *Adv. Mater.* **2006**, *18*, 461. (22) Garcia-Santamaria, F.; Xu, M.; Lousse, V.; Fan, S.; Braun, P.V.; Lewis, J.A. *Adv. Mater.* **2007**, *19*, 1567.

Micro- and Nanoscale Powders

The following table gives a short selection of ceramic and metal particulate materials suitable for formulating inks for 3D direct writing of ceramic and metal structures.

For a complete list of available ceramics, visit ***sigma-aldrich.com/ceramics***.
For a complete list of available metal nanoparticles, visit ***sigma-aldrich.com/nano***.

Name	Physical Form	Particle Size	Powder Purity / Dispersion Concentration	Prod. No.
Aluminum oxide				
(alumina, Al_2O_3)	Powder	–100 mesh	99.9%	**319767-25G**
				319767-100G
		10 µm (average)	99.7%	**265497-25G**
				265497-500G
				265497-2.5KG
	Nanopowder	< 50 nm (BET)		**544833-10G**
				544833-50G
	Dispersion	< 50 nm (BET)	10 wt.% in H_2O, pH 5–7	**642991-100ML**
Silicon dioxide				
(silica, SiO_2)	Powder	–325 mesh	99.6%	**342890-100G**
				342890-1KG
		0.5–10 µm	~ 99%	**S5631-100G**
				S5631-500G
				S5631-1KG
	Nanopowder	10–20 nm (BET)	99.5%	**637238-50G**
				637238-250G
				637238-500G
		5–15 nm (BET)	99.5%	**637246-50G**
				637246-250G
				637246-500G
	Dispersion (LUDOX™ HS-40)	12 nm (average)	40 wt.% in H_2O, pH 9.8	**420816-1L**
				420816-4L
				420816-18L
	Dispersion (LUDOX™ TM-50)	22 nm (average)	50 wt.% in H_2O, pH 9.0	**420778-1L**
				420778-4L
				420778-18L
	Dispersion 5–10 wt.% alumina doped	< 50 nm (BET)	10 wt.% in H_2O	**643084-100ML**
				643084-500ML
Piezoelectric Ceramics				
Barium titanate(IV) ($BaTiO_3$)	Powder	2 µm (average)	99.9%	**338842-100G**
				338842-500G
	Nanopowder	30–50 nm	99+%	**467634-25G**
				467634-100G
Lead(II) titanate ($PbTiO_3$)	Powder	< 5 mm	≥ 99%	**215805-250G**

For questions, product data, or new product suggestions, please contact Aldrich Materials Science at matsci@sial.com.

Biocompatible Ceramics				
Hydroxyapatite ($Ca_5(OH)(PO_4)_3$), synthetic	Powder		99.999%	**574791-5G** **574791-15G**
	Nanopowder	< 200 nm (BET)	97+%	**677418-5G** **677418-10G**
	Nanopowder, 5% silica doped	< 200 nm (BET)		**693863-5G**
Calcium phosphate ($Ca_2O_7P_2$), amorphous	Nanopowder	< 100 nm (BET)		**693871-5G**
β-Tricalcium phosphate ($Ca_3O_8P_2$)	Powder		≥ 98%	**13204-10G** **13204-100G**
Tricalcium phosphate ($Ca_3(PO_4)_2$)	Nanopowder	< 200 nm (BET)		**693898-5G**
Metal Nanopowders				
Copper (Cu)	Nanopowder	< 100 nm	99.8%	**634220-25G** **634220-100G**
		< 50 nm (TEM)	99.9+%	**684007-25G**
Palladium (Pd)	Nanopowder	< 25 nm (TEM)	99.9+%	**686468-500MG**
Silver (Ag)	Nanopowder	< 100 nm	99.50%	**576832-5G**
	Dispersion	< 100 nm (TEM)	10 wt.% in ethylene glycol	**658804-5G** **658804-25G**
Platinum (Pt)	Nanopowder	< 50 nm (BET)	99.9+%	**685453-500MG**
Gold (Au)	Nanopowder	< 100 nm	99.9+%	**636347-1G**

Polyelectrolytes

In addition to inks for 3D direct writing, the following polyelectrolytes can be used for two other important 3D patterning techniques: layer-by-layer (LbL) self-assembly (see Ref. 10 in article on p. 10) and nanofiber electrospinning (see article on p. 19). Generally, smaller molecular weights ($M_w \lesssim 100{,}000$) are used for 3D-Inks, where lower solution viscosities are preferred. Higher M_w polyelectrolytes are usually used for electrospinning, although the technique will work with lower molecular weight polymers, if they are cross-linked or gelled. For a complete list of polyelectrolytes and latest products, visit ***sigma-aldrich.com/polymer***.

Name	Structure	Molecular Weight	Prod. No.
Anionic Polyelectrolytes			
Poly(anetholesulfonic acid, sodium salt)	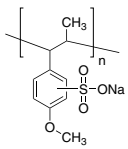	Avg. M_v 9,000–11,000	**444464-5G** **444464-25G**
Poly(sodium 4-styrenesulfonate)	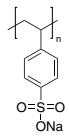	Avg. M_w ~ 70,000	**243051-5G** **243051-100G** **243051-500G**
		Avg. M_w ~ 1,000,000	**434574-5G** **434574-100G** **434574-500G**
Poly(4-styrenesulfonic acid),	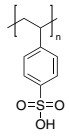	M_w ~ 75,000, 18 wt. % in H_2O	**561223-100G** **561223-500G**
Poly(4-styrenesulfonic acid-*co*-maleic acid)	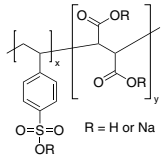	Avg. M_w ~ 20,000, *x*:*y* = 1:1	**434558-250G** **434558-1KG**
		Avg. Mw ~ 20,000, *x*:*y* = 3:1	**434566-250G** **434566-1KG**

TO ORDER: Contact your local Sigma-Aldrich office (see back cover), or visit sigma-aldrich.com/matsci.

Poly(vinylphosphonic acid)		Variable M_w	**661740-1G**
Poly(vinyl sulfonate), potassium salt		Avg. M_w ~ 170,000	**271969-1G** **271969-5G**
Poly(acrylic acid)	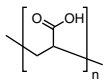	Avg. M_w ~ 1,800	**323667-5G** **323667-100G** **323667-250G**
		Avg. M_v ~ 450,000	**181285-5G** **181285-100G** **181285-250G**
		Avg. M_v ~ 1,250,000	**306215-5G** **306215-100G** **306215-250G**
		Avg. M_v ~ 4,000,000	**306231-5G** **306231-100G** **306231-250G**
Poly(acrylic acid, sodium salt)		Avg. M_w ~ 2,100	**420344-100G** **420344-500G**
		Avg. M_w ~ 5,100	**447013-100G** **447013-500G**
Cationic Polyelectrolytes			
Poly(allylamine hydrochloride)	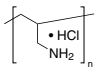	Avg. M_w ~ 15,000 (vs. PEG std.)	**283215-5G** **283215-25G**
		Avg. M_w ~ 70,000 (vs. PEG std.)	**283223-1G** **283223-5G** **283223-25G**
Poly(diallyldimethylammonium chloride)	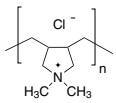	Avg. M_w < 100,000 very low molecular weight, 35 wt. % in H_2O	**522376-25ML** **522376-1L**
		Avg. M_w 100,000–200,000 low molecular weight, 20 wt. % in H_2O	**409014-25ML** **409014-1L** **409014-4L**
		Avg. M_w 400,000–500,000 high molecular weight, 20 wt. % in H_2O	**409030-25ML** **409030-1L** **409030-4L**
Polyethylenimine	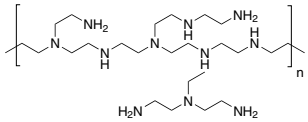	Avg. M_w ~ 1,300 (by LS), 50 wt. % in H_2O	**482595-100ML** **482595-250ML**
		Avg. M_w ~ 25,000 (by LS), branched	**408727-100ML** **408727-250ML** **408727-1L**
		Avg. M_w ~ 750,000 (by LS), 50 wt. % in H_2O	**181978-5G** **181978-18KG** **181978-100G** **181978-250G**
Polyethylenimine, 80% ethoxylated, 35–40 wt. % in H_2O	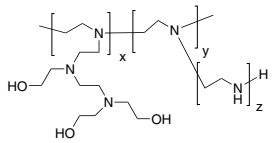	Avg. M_w ~ 70,000, 35–40 wt. % in H_2O	**423475-50ML** **423475-250ML**

From Form to Function: Molding Porous Materials in Three Dimensions by Colloidal Crystal Templating



Melissa A. Fierke, Fan Li, and Prof. Andreas Stein

Department of Chemistry, University of Minnesota

Overview

Methods of structuring materials with submicrometer features in two dimensions have become highly sophisticated. For example, lithographic methods are now capable of carving out several hundred million electronic components on an integrated circuit the width of a fingernail. Extending similar architectures into the third dimension by using these top-down engineering methods is possible only to a limited degree and at great expense. Bottom-up chemical methods involving self-assembly and templating provide promising alternatives to 3D structures with critical dimensions on the length scale of nanometers to micrometers. One such approach, colloidal crystal templating, is particularly versatile, and has been demonstrated for materials that target applications such as photonic crystals, sensors, power storage devices, artificial bone materials and multifunctional catalysts.[1]

A colloidal crystal is an ordered array of particles with diameters ranging from tens of nanometers to micrometers. In typical templating syntheses, these are arrangements of close-packed, uniformly sized polymer or silica spheres. Such colloidal crystals resemble natural opals, both in their geometries (face-centered cubic sets of spheres) and in their beautiful opalescent appearances caused by diffraction of light. In both cases, the interstitial volume between the spheres can be filled with a second phase. When colloidal crystals are used as a template, the original spheres are then removed, leaving an inverse replica of the opal structure, known as an inverse opal or three-dimensionally ordered macroporous (3DOM) structure (**Figure 1**). These structures consist of solid walls surrounding an ordered array of spherical voids with windows connecting the pores where template spheres were in contact (**Figure 2**). The walls are typically tens of nanometers thick, while the void sizes depend on the diameter of the template spheres.

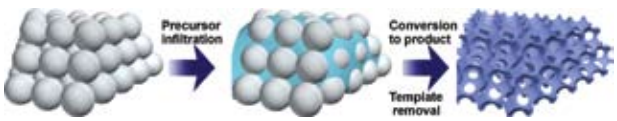

Figure 1. Scheme of the general colloidal crystal templating process. A colloidal crystal is infiltrated by a precursor material, followed by conversion of the precursor to the final product and sphere removal.

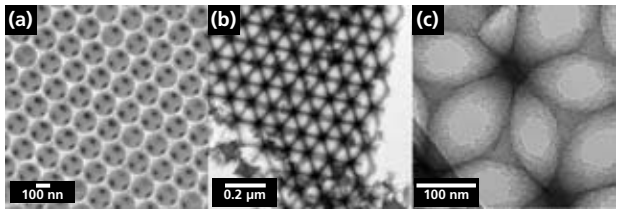

Figure 2. (a) Scanning electron micrograph of a 3DOM carbon monolith showing the periodic porosity of the structure. Dark circles are windows between the pores. (b, c) Transmission electron micrographs of 3DOM silica. The light areas correspond to the macropores space. In the higher resolution image (c) additional mesopore channels are visible within the wall structure.

Porous nanostructures synthesized by colloidal crystal templating can offer several advantages over porous materials made by other methods. Unlike materials produced using less regular templates, inverse opals are highly periodic in three dimensions. Changing the size of the spheres in the colloidal crystal template easily controls pore sizes. Inverse opals typically have relatively large surface areas, and the open structure offers easy access to the entire surface. These materials have continuous wall skeletons with thicknesses on the order of nanometers, so they can exhibit some properties of nanoparticles, including confinement effects and high surface-to-volume ratios.[2] Also, the synthesis methods for inverse opal materials are quite versatile, producing materials of various compositions and morphologies with a wide range of pore sizes, which are being investigated for many distinct applications (see **Table 1**).

Table 1. Potential applications of 3DOM materials and benefits provided by the inverse opal structures.[2]

Application	Benefits of 3DOM Material
Photonic crystals	Periodicity on length scale of visible and infrared light, cheap preparation
Pigments	Tunable color based on pore size, stability to light, chemical stability, no toxic components required
Optical sensors	In 3DOM hydrogels, colors change with changes in pore sizes as a function of temperature, humidity, solvent, etc.
Electrochemical sensors	High signal stability demonstrated for 3DOM carbon, no light interference
Lithium ion batteries	Short ion diffusion paths, high rate capability, potential for high power density in small footprint applications
Supercapacitors	High surface areas in 3DOM materials with hierarchical pore structure
Bioglasses	Fast conversion of 3DOM bioglass to bone-like hydroxyapatite due to easily accessible large surface area
Catalysts	High throughput permits short contact time, no significant pressure build-up, possibility of combining multiple catalytic components in one material
Interfacial materials	Tunable wettability from hydrophilic to superhydrophobic

Preparing the Colloidal Crystal Template

The colloidal crystal templates are formed by packing monodisperse spheres into close-packed arrays. Typically, silica spheres are synthesized by variations of the Stöber-Fink-Bohn method,[3] while polymer, poly(methyl methacrylate) (PMMA) or poly(styrene) (PS) spheres are made by emulsion polymerization,[4,5] with or without added emulsifier (see Sphere Preparation Note on p. 13). Spheres ranging in size from tens of nm to hundreds of µm can be employed. A partial list of the possible methods to order spheres into colloidal crystal templates includes gravity sedimentation, centrifugation, filtration, two-dimensional deposition, slit fitting, and pressing.[6] The most common packing arrangement is based on hexagonally close packed (hcp) layers and face-centered cubic (fcc) packing which provides nearly one quarter of the template volume as interstitial space available for subsequent infiltration.

The Templating Process

Most colloidal crystal templating processes involve three general steps. First, a precursor material is infiltrated into the void spaces of the colloidal crystal template. Next, the precursor is converted into the desired solid product. Finally, to create the porosity within the sample, the spheres are removed during or after precursor conversion (Figure 1). The technique is quite versatile and is used with many types of precursor materials. Some of the reported synthesis techniques include sol-gel, infiltration with a metal salt, solvothermal synthesis, electrochemical deposition, electroless deposition, chemical vapor deposition, melt imbibing, and organic polymerization.[1] Porous silicates can be made using the sol-gel method with tetraethoxysilane (**333859**) or tetramethoxysilane (**679259**). Other oxides prepared by sol-gel methods include those of Ti, Zr, Al, W, Fe, and Sb. Additional elements can be incorporated by subsequent doping or by employing mixed metal precursors or alkoxide/acetate mixtures. For example, yttria-stabilized zircionia can be made from a mixture of zirconium *n*-propoxide (**333972**) and yttrium tri-isopropoxide (**665916**).[7] Templated precipitation of metal salts (acetates, oxalates, etc.) provides a route to macroporous oxides, metals, and metal carbonates. For example, periodic macroporous hematite (Fe_2O_3) was made by 3DOM templating using an aqueous solution of iron (III) oxalate (**381446**).[8] The 3DOM Ni_xCo_{1-x} alloy was templated from a PMMA array using methanol solutions of nickel(II) acetate (**379883**) and cobalt (II) acetate (**437875**).[9] In this case, metal oxalates were formed by soaking PMMA-salt composites in oxalic acid (**658537**) solution, followed by processing at 400 °C in a reducing atmosphere.

Another option is co-deposition of nanoparticles with the colloidal crystal spheres. After the nanoparticles settle within the array of spheres, they can be sintered to form a continuous skeleton. Co-deposition is typically used when nanoparticles of the desired product phase are easier to synthesize *ex-situ* than within the confinement of the template. The third technique currently used to produce inverse opal materials involves core-shell materials that are assembled into ordered arrays. After the spheres are removed, the remaining material consists of hollow close-packed shells. Macroporous titania was produced by this method by coating PS spheres with polyelectrolyte multilayers infiltrated with titanium (IV) isopropoxide (**377996**).[10]

Following infiltration of the colloidal crystals, the precursor materials must be converted to the desired products. This can be accomplished by drying, pyrolysis or calcination, chemical conversion, crosslinking, cooling, etc., depending on the precursor materials used. In order to create the characteristic porosity in the inverse opal structure, the template spheres need to be eliminated. If polymer spheres are utilized as the template, they are typically removed by combustion, which may coincide with thermal conversion of the precursor. Polymer spheres can also be removed by solvent extraction. Silica spheres are typically removed by etching with a strong base or hydrofluoric acid.

The Compositional Spectrum

Because of the versatility of this templating method, possible product compositions are bounded largely by our imagination. One of the few restrictions is that the product must be able to withstand template removal without being damaged or deformed. The first inverse opals synthesized were simple oxides, including titania, zirconia, alumina, and silica.[11–13] Since then, many oxides have been prepared, including more simple oxides, as well as ternary and mixed oxides with much more complicated compositions. Non-oxides, such as carbon have also been synthesized. Various allotropes of carbon have been created with inverse opal structures, including graphitic, diamond, and glassy carbons.[14,15] Other non-oxides include various carbides, nitrides, and chalcogenides. For example, the 3DOM chalcogenide CdS was prepared galvanostatically in silica opals from DMF or DMSO solutions of sulfur (**213292**) and $CdCl_2$ (**202908**).[1] Metallic and semiconducting macroporous materials are other classes of inverse opals that have been created. Macroporous gold was prepared from solutions of 15–21 nm colloidal gold (e.g. **G1652**), and the 3DOM semiconductor CdSe was made from solutions of CdSe nanocrystals (e.g. **662550**).

Polymeric 3DOM materials can also be synthesized, including hydrocarbon polymers, as well as conducting and semiconducting polymers. Polymeric 3DOMs can be made either by templating monomer solution, or by filling colloidal crystals with solutions of preformed polymers. Electrodeposition or oxidative polymerization was used to prepare 3DOM conducting polymers, such as poly(pyrrole), poly(aniline), and poly(bithiophene) from pyrrole (**131709**), aniline (**242824**), and bithiophene (**241636**), respectively.[1] Inverse opal hydrogels that respond to external stimuli, including pH, temperature, humidity, and the surrounding chemical environment have been developed. By combining multiple synthesis techniques or through functionalization of the finished structures, inverse opal materials with hybrid organic-inorganic compositions are possible.

Tuning Morphologies

Product structures can be controlled at both nanometer and bulk length scales by choosing appropriate forms of the template and the precursors. Changes in the colloidal crystal packing method and synthesis techniques have been used to create products of varying morphologies, including monolithic materials, powders, thin films, and wires, all with long-range, ordered porosity. By adding secondary templates, such as block-copolymers or surfactants, it is possible to introduce smaller mesopores into the walls that surround the macropores formed by the colloidal particles.[16] Such hierarchical porosity introduces extremely large surface areas while keeping diffusion paths short and surfaces readily accessible. Recently, dual templating processes have even been used to create porous nanoparticles with specific shapes (cubes, tetrapods, spheres).[17] A few examples of these materials are shown in **Figure 3**.

ALDRICH Chemistry

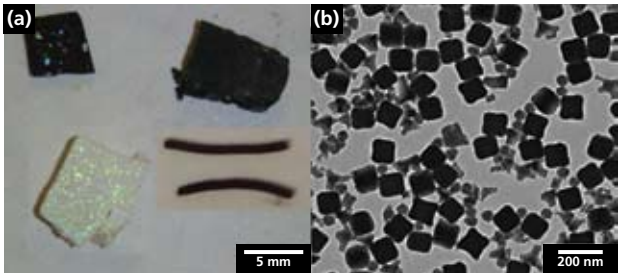

Figure 3. Examples of possible morphologies of materials prepared by colloidal crystal templating: (a) inverse opal monoliths composed of carbon (top left), tungsten (top right), and silica (bottom left). 3DOM carbon filaments are also shown (bottom right). (b) Mesoporous silica nanocubes, spheres and tetrapods prepared by dual templating with both colloidal crystals and surfactants.

From Form to Function

Inverse opals are being investigated for a wide range of applications because of their unique properties. The highly periodic structure with repeat distances coinciding with the wavelength of visible or infrared light, makes them desirable as photonic crystals that can guide and manipulate light.[18,19] 3DOM materials are also being examined for use as sensors because they can give a measurable response to different stimuli, including a change in refractive index, a change in pore spacing or geometry, or a change in surface electronic states.[20,21] They are being considered for electrochemical power systems, including an early development of a nanostructured Li-ion battery with interpenetrating anode, electrolyte and cathode components—a paradigm shift in battery architectures intended for small devices with little available footprint area for a power source.[22] Another possible application of these materials is their use as non-toxic, color-fast pigments that can be prepared with any color of the spectrum, depending on the composition of the material, the pore size within the structure, and the refractive index of the material filling the pores (**Figure 4**). Such pigments can even change their colors reversibly, if pores are filled with a liquid.[23] Reactive applications that take advantage of the large surface area of 3DOM materials and ready access to the pores include complex catalyst supports and bioglasses for bone repair.[24]

Figure 4. Photographs of 3DOM zirconia, silica (top middle) and titania powders (bottom left). The different colors of the 3DOM zirconia samples arise from the different pore sizes.

The Bottom Line

Colloidal crystal templating is a simple, highly versatile synthetic technique for creating periodic structures with nanometer-to-submicrometer features in three dimensions. It is used to synthesize highly ordered porous materials with a wide range of pore sizes, morphologies, and compositions. The inverse opal products are being investigated by scientists around the world for a variety of applications, where they can provide features and functionalities that are either difficult to obtain by other methods or (in the case of 3D photonic crystals) much less expensive than alternative techniques. As the field of colloidal crystal templating continues to grow, more unique materials and applications are sure to be developed.

References:

(1) Stein, A.; Schroden, R. C. *Curr. Opin. Solid St. Mater. Sci.* **2001**, *5*, 553–564 and references therein. (2) Lytle, J. C.; Stein, A., Recent Progress in Syntheses and Applications of Inverse Opals and Related Macroporous Materials Prepared by Colloidal Crystal Templating. In *Annual Reviews of Nano Research*, Cao, G.; Brinker, C. J., Eds. World Scientific Publishing Co.: New Jersey, 2006; Vol. 1, pp 1–79 and references therein. (3) Stöber, W.; Fink, A.; Bohn, E. *J. Colloid Interface Sci.* **1968**, *26*, 62. (4) Goodwin, J. W.; Hearn, J.; Ho, C. C.; Ottewill, R. H. *Br. Polym. J.* **1973**, *5*, 347. (5) Tanrisever, T.; Okay, O.; Sonmezoglu, I. C. *J. Appl. Polym. Sci.* **1996**, *61*, 485. (6) Velev, O. D.; Lenhoff, A. M. *Current Opinion in Colloid & Interface Science* **2000**, *5*, 56. (7) Holland, B.T.; Blanford, C.F.; Do, T.; Stein, A. *Chem Mater.* **1999**, *11*, 795. (8) Yan, H.; Blanford, C.F.; Holland, B.T.; Smyrl, W.H.; Stein, A. *Chem Mater.* **2000**, *12*, 1134. (9) Yan, H.; Blanford, C.F.; Smyrl, W.H.; Stein, A. *Chem. Commun.* **2000**, 1477. (10) Wang, D.; Caruso, R.A..; Caruso, F. *Chem Mater.* **2001**, *13*, 364. (11) Velev, O. D.; Jede, T. A.; Lobo, R. F.; Lenhoff, A. M. *Nature* **1997**, *389*, 447. (12) Holland, B. T.; Blanford, C. F.; Stein, A. *Science* **1998**, *281*, 538. (13) Wijnhoven, J. E. G. J.; Vos, W. L. *Science* **1998**, *281*, 802. (14) Zakhidov, A. A.; Baughman, R. H.; Iqbal, Z.; Cui, C.; Khayrullin, I.; Dantas, S. O.; Marti, J.; Ralchenko, V. G. *Science* **1998**, *282*, 897. (15) Wang, Z.; Stein, A. *Chem. Mater.* **2008**, *20*, DOI 10.1021/cm0717864. (16) Li, F.; Wang, Z.; Ergang, N. S.; Fyfe, C. A.; Stein, A. *Langmuir* **2007**, *23*, 3996. (17) Li, F.; Wang, Z.; Stein, A. *Angew. Chem. Int. Ed.* **2007**, *46*, 1885. (18) Blanco, A.; Chomski, E.; Grabtchak, S.; Ibisate, M.; John, S.; Leonard, S. W.; Lopez, C.; Meseguer, F.; Miguez, H.; Mondia, J. P.; Ozin, G. A.; Toader, O.; van Driel, H. M. *Nature* **2000**, *405*, 437. (19) Vlasov, Y. A.; Bo, X. Z.; Sturm, J. C.; Norris, D. J. *Nature* **2001**, *414*, 289. (20) Lee, Y.-J.; Heitzman, C. E.; Frei, W. R.; Johnson, H. T.; Braun, P. V. J. *Phys. Chem. B* **2006**, *110*, 19300. (21) Barry, R. A.; Wiltzius, P. *Langmuir* **2006**, *22*, 1369. (22) Ergang, N. S.; Lytle, J. C.; Lee, K. T.; Oh, S. M.; Smyrl, W. H.; Stein, A. *Adv. Mater.* **2006**, *18*, 1750. (23) Blanford, C. F.; Schroden, R. C.; Al-Daous, M.; Stein, A. *Adv. Mater.* **2001**, *13*, 26. (24) Yan, H.; Zhang, K.; Blanford, C. F.; Francis, L. F.; Stein, A., *Chem. Mater.* **2001**, *13*, 1374.

Application Note:

Preparation of Monodisperse Polymer Spheres

Melissa A. Fierke, University of Minnesota

Monodisperse, surfactant-free polymer spheres for use as colloidal crystal templates can be easily obtained in reasonably large quantities. Typical synthesis methods for poly(methyl methacrylate) (PMMA) and poly(styrene) (PS) by emulsifier free emulsion polymerization are described below and yield spheres several hundred nanometers in diameter. Sphere sizes can be adjusted by altering the stirring rate, monomer concentration, reaction temperature, and amount of initiator. In both cases, the reaction is carried out in a four-necked round-bottom flask equipped with an electric stirrer with a Teflon stir blade, a water condenser, a pipet connected to a source of nitrogen, and a thermocouple probe (**Figure 1a**).

To synthesize PMMA spheres, 1600 mL of deionized water and 400 mL of methyl methacrylate (**M55909**) monomer are added to the flask. The mixture is stirred at approximately 350 rpm and bubbled with nitrogen. The temperature is increased to 70 °C and the system is allowed to equilibrate. After temperature stabilization, 1.50 g of the initiator, 2,2′-azobis (2-methylpropionamidine) dihydrochloride (**440914**), is dissolved in approximately 25 mL of deionized water and added to the flask (Figure 1b). Within several minutes, the mixture in the flask turns milky white. Over the course of the reaction (1–2 hours), the temperature rises several degrees before returning to 70 °C, signaling the end of the reaction.

The synthesis of PS spheres is very similar. 1700 mL of deionized water is added to the flask and heated to 70 °C while stirring at about 350 rpm. After the temperature has stabilized, 200 mL of washed styrene (**240869**) is added, and the temperature is allowed to equilibrate. Next, 0.663 g of the initiator, potassium persulfate (**379824**), is dissolved in 100 mL of water and heated to 70 °C before addition to the flask. The temperature is held constant, and the mixture is stirred for 28 hours.

After the polymerization reactions are complete, the polymer sphere solutions are filtered through glass wool to remove any large agglomerates from the solution. The spheres are then ordered into a colloidal crystal (Figure 1c) by one of several methods described in the text of article on p. 10 of this issue.

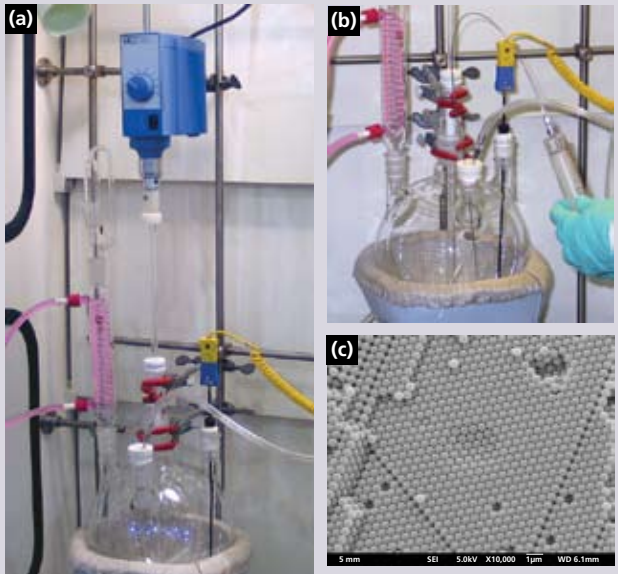

Figure 1. (a) Photograph of reactor setup for preparation of monodisperse polymer spheres. Please refer to the Product Table for list of reactor components. (b) Reagents (e.g. free-radical initiators) are added to the reaction via syringe without breaking N_2 atmosphere inside the reactor. (c) SEM image of a typical PMMA colloidal crystal with multiple layers of monodisperse PMMA spheres packed in fcc structure. Point and line defects often observed in these colloidal crystals are also visible in the micrograph.

Components for Reactor Setup

Description	Prod. No.
Flask, round-bottom, 4-neck, 34/45 center, 24/40 side joints	Z561096-1EA
Bubbler, 24/40 joint	Z104329-1EA
Condenser, coiled, 300 mm L, 24/40 joints	Z552356-1EA
Septa, for 24/40 joints	Z553980-10EA
Mixer, model RW 16, 115 V	Z403881-1EA
Stirrer bearing, PTFE, for 10 mm o.d. shaft, 34/45 joint	Z555614-1EA
Stirrer blade, PTFE, fits 10 mm o.d. shaft, 125 mm W	Z105740-1EA
Stirrer chuck, fits 10 mm o.d. shaft	Z136786-1EA
Stirrer shaft, polished, 10 mm o.d. x 580 mm L, with button	Z136735-1EA
Syringe needle, 304 SS, Luer connector, non-coring point, 18 gauge, 2 in. L, for nitrogen gas	Z113042-1EA
Syringe needle, 304 SS, Luer connector, non-coring point, 18 gauge, 24 in. L, for cannulation	Z100862-1EA
Syringe, 30 mL, metal Luer tip	Z181269-1EA
Needle-tubing connector, for 1/4 in. — 5/16 in. i.d. tubing, Luer connector	Z101168-4EA
Heating mantle, hemispherical, for 5 L flasks, 115 V	Z284890-1EA
Temperature controller, J-KEM® model 210, 120 V*	Z210226-1EA
Adapter, thermocouple probe, PTFE, 1/8 in. i.d. hole, 24/40 joint for J-KEM temperature controller	Z248282-1EA

*Includes Type T thermocouple probe shown in Figure 1a,b
J-KEM is a registered trademark of J-KEM Scientific, Inc.

ALDRICH Chemistry

Sol-Gel Precursors

Sol-gel chemistry employing alkoxide, acetylacetonate (acac) and acetate precursors provides a convenient route to 3-dimensionally structured metal oxide materials. The chemistry is versatile both in terms of compatibility with all major nano- and micropatterning techniques described in this issue, as well as variety of available precursors, spanning the periodic table. The product table below groups sol-gel precursors by metal and can be used as a selection tool for synthesis of simple and mixed oxide materials.
For example, titanium butoxide (**244112**) can be combined with barium acetate (**255912**) or lead acetate (**398845**) to make piezoelectrics $BaTiO_3$ and $PbTiO_3$.[1,2]

For a complete list of sol-gel precursors, unit sizes, and prices, visit ***sigma-aldrich.com/solgel***.

Element	Name	Purity (%)	Prod. No
3: Li	Lithium acetate	99.99	517992
	Lithium acetate dihydrate	99.999	450189
	Lithium acetylacetonate	97	413046
	Lithium ethoxide	95	400203
	Lithium isopropoxide	95	348937
	Lithium methoxide	98	344370
	Lithium *tert*-butoxide	97	400173
4: Be	Beryllium acetylacetonate	97	522791
5: B	Triethyl borate	99	T59307
	Triisopropyl borate	98+	197335
	Tripropyl borate	98	224928
	Tri-*tert*-butyl borate	98	236608
11: Na	Sodium acetate	99.995	229873
	Sodium 2-ethylhexanoate	97	511692
	Sodium phenoxide trihydrate	99	318191
	Sodium *tert*-butoxide	97	359270
	Sodium *tert*-pentoxide	95	280704
12: Mg	Magnesium acetate tetrahydrate	99.999	229768
	Magnesium acetylacetonate dihydrate	98	129577
	Magnesium ethoxide	98	291846
	Magnesium trifluoroacetylacetonate hydrate		103225
13: Al	Aluminum acetylacetonate	99	208248
	Aluminum ethoxide	97	235857
	Aluminum isopropoxide	99.99+	229407
	Aluminum phenoxide	99.9	495131
	Aluminum *tert*-butoxide, technical grade		235849
	Aluminum-tri-*sec*-butoxide	99.99	511609
	Diethylaluminum ethoxide	97	256749
14: Si	Tetraethyl orthosilicate (TEOS)	99.999	333859
	Tetramethyl orthosilicate (TMOS)	98+	679259
	Tetrapropyl orthosilicate	98+	679240
15: P	Triethyl phosphite	98	T61204
19: K	Potassium acetate	99.98	255785
	Potassium ethoxide	95	333379
	Potassium methoxide	95	292788
20: Ca	Calcium acetate hydrate	99.99	379964
	Calcium acetylacetonate hydrate	99.95	C107
	Calcium isopropoxide, powder	99.9+	497398
	Calcium methoxide	97	445568
21: Sc	Scandium(III) acetate hydrate	99.9	325899
	Scandium(III) acetylacetonate hydrate		556904
	Scandium(III) isopropoxide		410128

Element	Name	Purity (%)	Prod. No
22: Ti	Titanium diisopropoxide bis(acetylacetonate)		325252
	Titanium(IV) butoxide	97	244112
	Titanium(IV) isopropoxide	99.999	377996
	Titanium(IV) methoxide	99.99+	463582
	Titanium(IV) oxide acetylacetonate		330833
	Titanium(IV) propoxide	98	253081
	Titanium(IV) *tert*-butoxide		462551
	Titanium(IV) tetrahydrofurfuryloxide		517038
23: V	Vanadium(V) oxytriethoxide	95	470775
	Vanadium(V) oxytriisopropoxide		404926
	Vanadium(V) oxytripropoxide	98	470783
	Vanadyl acetylacetonate	99.99	574562
24: Cr	Chromium(III) acetylacetonate	99.99	574082
	Chromium(III) trifluoroacetylacetonate	99.9+	495697
25: Mn	Manganese(II) acetate	98	330825
	Manganese(II) acetylacetonate		245763
26: Fe	Iron(II) acetate	99.995	517933
	Iron(II) acetylacetonate	99.95	413402
	Iron(III) acetylacetonate	99.9+	517003
27: Co	Cobalt(II) acetate	99.995	399973
	Cobalt(III) acetylacetonate	99.99+	494534
28: Ni	Nickel(II) acetate tetrahydrate	99.998	379883
	Nickel(II) acetylacetonate	95	283657
29: Cu	Copper(I) acetate	97	403342
	Copper(II) acetate	99.999	517453
	Copper(II) acetylacetonate	99.99+	514365
	Copper(II) methoxide	97	332666
	Copper(II) trifluoroacetylacetonate	97	101826
30: Zn	Zinc acetate	99.99	383317
	Zinc acetylacetonate hydrate	99.995	480991
31: Ga	Gallium(III) acetylacetonate	99.99	393541
32: Ge	Germanium(IV) ethoxide	99.95+	339180
	Germanium(IV) isopropoxide	97	447641
	Germanium(IV) methoxide	97	396362
37: Rb	Rubidium acetate	99.8+	289302
	Rubidium acetylacetonate		392618
38: Sr	Strontium acetate hydrate	99.995	437883
	Strontium acetylacetonate	97	390720

TO ORDER: Contact your local Sigma-Aldrich office (see back cover), or visit sigma-aldrich.com/matsci.

Element	Name	Purity (%)	Prod. No
39: Y	Yttrium isopropoxide oxide		379425
	Yttrium(III) acetate hydrate	99.9	326046
	Yttrium(III) acetylacetonate hydrate	99.95	438790
	Yttrium(III) butoxide, solution, 0.5 M in toluene	99.9+	510661
	Yttrium(III) isopropoxide, solution, 25 wt. % in toluene		380296
40: Zr	Zirconium(IV) acetylacetonate	98	338001
	Zirconium(IV) bis(diethyl citrato)dipropoxide		515817
	Zirconium(IV) butoxide, 80 wt. % in 1-butanol		333948
	Zirconium(IV) ethoxide, 97%	97	339121
	Zirconium(IV) isopropoxide isopropanol complex	99.9	339237
	Zirconium(IV) propoxide, 70 wt. % in 1-propanol		333972
	Zirconium(IV) tert-butoxide, electronic grade	99.999	560030
	Zirconium(IV) trifluoroacetylacetonate	97	383325
41: Nb	Niobium(V) ethoxide	99.95	339202
42: Mo	Molybdenum(II) acetate dimer	98	232076
44: Ru	Ruthenium(III) acetylacetonate	97	282766
45: Rh	(Acetylacetonato)(1,5-cyclooctadiene) rhodium(I)	99	335029
	Rhodium(II) acetate dimer	99.99+	482285
	Rhodium(III) acetylacetonate	97	282774
46: Pd	Palladium(II) acetate	99.98	379875
47: Ag	Silver acetate	99.99	204374
	Silver acetylacetonate	98	323489
48: Cd	Cadmium acetate hydrate	99.99+	229490
	Cadmium acetylacetonate hydrate	99.9+	517585
49: In	Indium(III) acetate	99.99	510270
	Indium(III) acetylacetonate	99.99+	I3300
	Indium(III) *tert*-butoxide solution, 5 % (w/v) in *tert*-butanol	99.9+	479721
50: Sn	Dibutyltin bis(acetylacetonate)	95	520586
51: Sb	Antimony(III) acetate	99.99	483265
	Antimony(III) ethoxide		213314
	Antimony(III) isopropoxide	98	470732
	Antimony(III) methoxide		538345
	Antimony(III) propoxide	98	470724
55: Cs	Cesium acetate	99.99	450154
56: Ba	Barium acetate	99.999	255912
	Barium acetylacetonate hydrate		339059
	Barium isopropoxide powder	99.9	449679
57: La	Lanthanum(III) acetate hydrate	99.99+	542083
57: La	Lanthanum(III) acetylacetonate hydrate		325759
58: Ce	Cerium(III) acetate hydrate	99.999	529559
	Cerium(III) acetylacetonate hydrate		381403
59: Pr	Praseodymium(III) acetylacetonate hydrate	99.9+	517674
	Praseodymium(III) isopropoxide		410144
60: Nd	Neodymium(III) acetate hydrate	99.9	325805
	Neodymium(III) acetylacetonate hydrate		460427
	Neodymium(III) isopropoxide	99.8	410101
62: Sm	Samarium(III) acetate hydrate	99.9	325872
	Samarium(III) acetylacetonate hydrate	99.9+	517666
63: Eu	Europium(III) acetylacetonate hydrate		393215
64: Gd	Gadolinium(III) acetate hydrate	99.9	325678
	Gadolinium(III) acetylacetonate hydrate	99.9	331716
65: Tb	Terbium(III) acetate hydrate	99.9	325929
	Terbium(III) acetylacetonate hydrate	99.9	484008
66: Dy	Dysprosium(III) acetate hydrate	99.99	325538
	Dysprosium(III) acetylacetonate hydrate	99.9	481491
67: Ho	Holmium(III) acetate hydrate	99.9	467332
68: Er	Erbium(III) acetylacetonate hydrate	97	483990
70: Yb	Ytterbium(III) acetate tetrahydrate	99.9	326011
	Ytterbium(III) isopropoxide	99.9	514063
71: Lu	Lutetium(III) acetate hydrate	99.9	325783
	Lutetium(III) acetylacetonate hydrate	99.9+	517658
72: Hf	Hafnium(IV) *tert*-butoxide	99.99	445541
	Tetrakis(1-methoxy-2-methyl-2-propoxy)hafnium(IV)	99.99	568171
77: Ir	(Acetylacetonato)(1,5-cyclooctadiene) iridium(I)		429155
	Iridium(III) acetylacetonate	97	333352
78: Pt	Platinum(II) acetylacetonate	99.99	523038
81: Tl	Thallium(I) acetylacetonate		153885
82: Pb	Lead(II) acetate trihydrate	99.999	316512
	Lead(IV) acetate	≥ 99.99	398845
83: Bi	Bismuth(III) acetate	99.99	401587

(1) Lei, Z.B.; Li, J.M.; Zhang, Y.G.; Lu, S.M. *J. Mater. Chem.* **2000**, *10*, 2629.
(2) Gundiah, G.; Rao, C.N.R. *Solid State Sci.* **2000**, *2*, 877.

ALDRICH Chemistry

Oxalate Salts

Templated precipitation of metal salts offers an alternative to classical sol-gel chemistry for synthesis of 3D structured materials. Oxalates are metal salts of oxalic acid with general structure $M_x(C_2O_4)_y$. Oxalates thermally decompose to give, depending on reaction conditions, structured metal oxides, carbonates, or metals, with gaseous (CO or CO_2) reaction byproducts.[1–4] Metal acetate hydrates (see Sol-Gel Precursors Table on p. 14) can be converted to corresponding metal oxalates in-situ during the templating process, by treatment with a solution of oxalic acid.[5]

Sigma-Aldrich® offers hundreds of additional metal salts for your materials chemistry work. For a complete list, unit sizes and prices visit ***sigmaaldrich.com/salts***.

Element	Name	Purity (%)	Prod. No.
11: Na	Sodium oxalate	99.99+	379735
19: K	Potassium oxalate monohydrate	99	223425
19: K	Potassium oxalate monohydrate	99.98	379727
20: Ca	Calcium oxalate	99.999	455997
20: Ca	Calcium oxalate hydrate		289841
20: Ca	Calcium oxalate monohydrate	98+	21201
21: Sc	Scandium(III) oxalate hydrate	99.99+	463833
22: Ti	Ammonium titanyl oxalate monohydrate	99.998	229989
22: Ti	Potassium titanium oxide oxalate dihydrate	90+	14007
24: Cr	Potassium chromium(III) oxalate trihydrate	98	311006
26: Fe	Ammonium iron(III) oxalate trihydrate	98+	12302
26: Fe	Iron(III) oxalate hexahydrate		381446
27: Co	Cobalt(II) oxalate dihydrate		401285
28: Ni	Nickel(II) oxalate dihydrate	99.999	463787
30: Zn	Zinc oxalate hydrate	99.99+	544957
38: Sr	Strontium oxalate	99.999	574163
41: Nb	Ammonium niobate(V) oxalate hydrate	99.99	525839
50: Sn	Tin(II) oxalate	98	402761
55: Cs	Cesium oxalate	99.9+	401277
56: Ba	Barium oxalate	99.999	456004
57: La	Lanthanum(III) oxalate hydrate	99.99	461024
58: Ce	Cerium(III) oxalate hydrate	99.999	574015
58: Ce	Cerium(III) oxalate hydrate	99.9	325511
59: Pr	Praseodymium(III) oxalate hydrate	99.9	325856
60: Nd	Neodymium(III) oxalate hydrate	99.99+	463817
63: Eu	Europium(III) oxalate hydrate	99.999	574228
64: Gd	Gadolinium(III) oxalate hydrate	99.9	325694
66: Dy	Dysprosium(III) oxalate hydrate	99.99+	463795
68: Er	Erbium(III) oxalate hydrate	99.9	325600
69: Tm	Thulium(III) oxalate	99.9+	587532
69: Tm	Thulium(III) oxalate hydrate	99.99+	463868
71: Lu	Lutetium(III) oxalate hydrate	99.99	480916

(1) Nagase, K.; Sato, K.; Tanaka, N. *Bull Chem. Soc. Jpn.* **1975**, *48*, 439.
(2) Mansour, S.A.A. *Thermochim. Acta* **1993**, *230*, 243.
(3) Dollimore, D.; Griffoths, D.L.; Nicholoson, D. *J. Chem. Soc.* **1963**, 2617.
(4) Robin, J. *Bull. Chim. France* **1953**, 1078.
(5) Yan, H.; Blanford, C.F.; Holland, B.T.; Smyrl, W.H.; Stein, A. *Chem. Mater.* **2000**, *12*, 1134.

Chemical Deposition Precursors

Sigma-Aldrich offers a complete line of precursors for thin-film deposition, surface modification and design of diverse nano-structures. Our current product offers include:

- High-purity metalorganics and metal salts
- High-purity metal alkyls, amides and alkoxides
- Metal acetylacetonates and related compounds
- Functionalized silanes and siloxanes
- Boron based materials and more

Functionalized siloxanes and Atomic Layer Deposition (ALD) precursors were featured in Material Matters™ Vol.1, No. 3.

Make Sigma-Aldrich Materials Science your one-stop source for Sol-Gel, ALD and CVD precursors — visit ***sigma-aldrich.com/matsci*** for latest products, technical publications, and the complete on-line product catalog.

Mesoporous Materials

Mespoporous materials, also known as mesoporous molecular sieves, are a class of 3D-nanostructures with well-defined mesoscale (2–50 nm diameter) pores and surface areas up to 1000 m^2/g.[1] In terms of characteristic ordered feature size, they occupy a unique place between crystalline zeolites and other types of 3D-structured materials described in this issue, e.g. 3DOM and direct-write materials with features > 100 nm. Mesoporous materials are formed by a self-assembly process from combined solutions of sol-gel precursors (e.g. metal alkoxides) and structure-directing amphiphiles, usually block-copolymers or surfactants (**Figure 1**).[2,3] Flexible, "one-pot synthesis" employing self-assembling templates enables the simultaneous control of size and 3D geometry (mesophase) of the pores. Furthermore, surface functionality of the pores can be modified by adding organically modified precursors, for example organosiloxanes $RSi(OR')_3$ or bis(organosiloxanes) $(R'O)_3Si\text{-}R\text{-}Si(OR')_3$, to the initial reaction mix.[4] On the other hand, it is relatively difficult to control long-range order and orientation of self-assembled structures and they typically have more defects and less structural precision compared to 3DOM or direct-write materials.

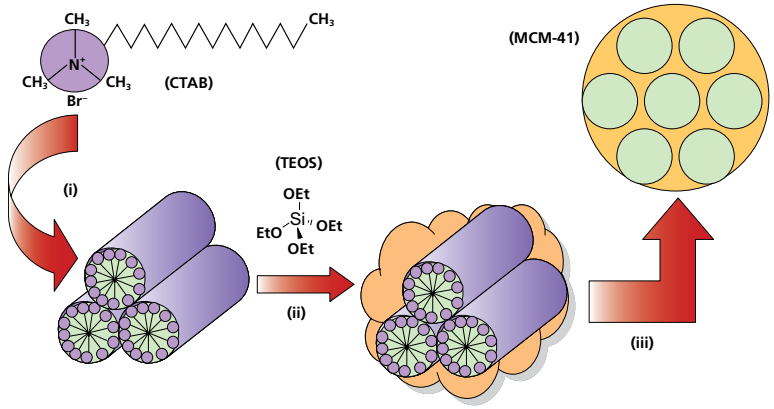

Figure 1. Schematic of the classical mesoporous silica (MCM-41) synthesis route.[2] **(i)** Surfactant, e.g. cetyltrimethylammonium bromide (CTAB, **52370**), is used to form liquid crystalline micelles in water. **(ii)** Ceramic sol-gel precursor, e.g. tetraethylorthosilicate (TEOS, **131903**), is added to this micellar solution to make, upon hydrolyses and condensation, a silica network around the micelles. **(iii)** Removal of the organic template by thermal treatment (calcination) or solvent extraction yields a mesoporous ceramic material, in this case hexagonally ordered MCM-41 silica framework.

Relative advantages of a given 3D-structure preparation route govern the resulting material applications. Ordered mesoporous materials templated by "soft" amphiphilic templates overcome pore size constraints of zeolites to allow more facile diffusion of bulky molecules. This lends them to applications in catalysis and absorption technologies where requirements for long-range material order can be less important. For example, acidic aluminosilicates are investigated for uses in fluid catalytic cracking and condensed-media chemical conversion processes.[5] Surface-functionalized mesoporous sieves can be used in active elements of sensors.[6] Large, optically active molecules, such as dyes[7] (e.g. rhodamine 6G **252433**) and conjugated polymers[8] (MEH-PPV **541443**) can be incorporated into mesoscale pores to make hybrid materials with unique optoelectronic properties.

Sigma-Aldrich® offers a number of mesoporous materials for your research, a selection of which is presented in the following **Mesoporous Materials** product tables (p. 18). In addition to the ready-made materials, we offer reagents for your own unique synthesis of mesoporous structures. The **Structure-Directing Amphiphiles** product table (p. 18) gives a short list of reagents commonly used as templates. Cationic quaternary ammonium surfactants are often used to prepare mesoporous silicates under basic hydrothermal conditions. Anionic surfactants are employed for aqueous synthesis of mesoporous alumina and for basic syntheses with added positively charged counterions or co-structure directing agents.[9,10] Nonioninc surfactants can be used to prepare disordered wormhole silicas (HMS, MSU) or ordered silicas under acidic conditions.[3] Highly ordered mesoporous materials with uniform pore sizes larger than 5 nm can be made with PEG-PPG-PEG[11] (Pluronic) triblock copolymers as templates in acidic aqueous media.[12] A broad choice of structure-directing surfactants and amphiphilic block-copolymers can be accessed using the Sigma-Aldrich online product catalog at ***sigma-aldrich.com/matsci***. Sol-gel precursors can be selected using the **Sol-Gel Precursors** Table on p. 14 of this issue, or browsed online at ***sigma-aldrich.com/solgel***.

References

(1) Beck, J.; Vartuli, J.C. *Curr. Opin. Solid State Mater. Sci.* **1996**, *1*, 76. (2) Beck, J. S.; Vartuli, J. C.; Roth, W. J.; Leonowicz, M. E.; Kresge, C. T.; Schmitt, K. D.; Chu, C. T. W.; Olson, D. H.; Sheppard, E. W.; McCullen, S. B.; Higgins, J. B.; Schlenker, J. L. *J. Am. Chem. Soc.* **1992**, *114*, 10834 (3) Wan, Y.; Zhao, D. *Chem. Rev.* **2007**, *107*, 2821. (4) For discussion of organofunctional siloxane chemistry, see Young, S.K. *Material Matters* **2006**, *1(3)*, 8. Solvent extraction methods, rather than calcinations, are usually required for template removal from functionalized mesostructures to prevent loss of organic functional groups. (5) Liu, Y.; Pinnavaia, T.J. *J. Mater. Chem.* **2002**, *12*, 3179. (6) Wirnsberger, G.; Scott, B. J.; Stucky, G. D. *Chem. Commun.* **2001**, 119–120. (7) Yang, P.; Wirnsberger, G.; Cordero, S.R.; Huang, H.C.; Scott, B.; McGehee, M.D.; Whitesides, G.M.; Chmelka, B.F.; Buratto, S.K.; Stucky, G.D. *Science* **2000**, *287*, 465. (8) Nguyen, T.Q.; Wu, J.; Tolbert, S.H.; Schwartz, B.J. *Adv. Mater.* **2001**, *13*, 609. (9) Huo, Q. S.; Margolese, D. I.; Ciesla, U.; Feng, P. Y.; Gier, T. E.; Sieger, P.; Leon, R.; Petroff, P. M.; Schuth, F.; Stucky, G. D. *Nature* **1994**, *368*, 317. (10) Che, S.; Garcia-Bennett, A. E.; Yokoi, T.; Sakamoto, K.; Kunieda, H.; Terasaki, O.; Tatsumi, T. *Nat. Mater.* **2003**, *2*, 801. (11) PPG = poly(propylene glycol); PEG = poly(ethylene glycol). (12) Zhao, D. Y.; Huo, Q. S.; Feng, J. L.; Chmelka, B. F.; Stucky, G. D. *J. Am. Chem. Soc.* **1998**, *120*, 6024.

Mesoporous Materials

For a complete list of mesoporous materials, including latest products, visit ***sigma-aldrich.com/nano***.

Name	Composition	Structure Type	Structure Dimensions	Prod. No.
Silica, mesostructured	SiO_2	MCM-41 hexagonal	4.6–4.8 nm unit cell size 2.3–2.7 nm pore size SSA ~1000 m^2/g (BET)	**643645-5G** **643645-25G**
		MSU-F cellular foam	~22 nm cell size ~15 nm cell window SSA ~562 m^2/g	**560979-10G**
		HMS wormhole	pore size 3.9 nm (avg.)	**541036-5G** **541036-25G**
		MSU-H large pore 2D hexagonal	~11.6 nm unit cell size ~7.1 nm pore size SSA ~750 m^2/g (BET)	**643637-5G** **643637-25G**
Aluminosilicate, mesostructured	SiO_2/Al_2O_3, ~3% aluminum	MCM-41 hexagonal	4.6–4.8 nm unit cell size 2.5–3 nm pore size SSA 940–1000 m^2/g (BET)	**643653-5G** **643653-25G**
		Al-MSU-F cellular foam	~22 nm cell size ~15 nm cell window SSA ~ 560 m^2/g	**643629-5G** **643629-25G**
Aluminum oxide, mesoporous	Al_2O_3	MSU-X wormhole	pore size 3.8 nm (avg.)	**517747-5G** **517747-25G**
			pore size 6.5 nm (avg.)	**517755-5G** **517755-25G**

Structure-Directing Amphiphiles

For package sizes and prices, please visit ***sigma-aldrich.com/matsci***.

Surfactants: $R\text{-}(CH_2)_{n-1}CH_3$

n\Head Group (–R)	$–N(CH_3)_3^+Br^–$	$–OSO_3^-Na^+$	$–CH_2COOH$	$–(OCH_2CH_2)_nOH$ (Brij®)*
8	**75091** (98%)	**75075** (95%)	**21410** (98%)	
10	**30725** (98%)		**L556** (98%)	
12	**44240** (98%)	**436143** (99%) SDS	**70080** (98.5%)	**235989** (n~4), **P1245** (n~23)
14	**87210** (98%)	**293938** (95%)	**258725** (99%)	
16	**52370** (98%) CTAB		**93661** (97%)	**388831** (n~2), **388858** (n~10) **16004** (n~20)
18	**359246** (98%)	**293946** (93%)	**A3631** (99%)	**388866** (n~2), **431281** (n~10) **436240** (n~20), **466387** (n~100)

*Brij is a registered trademark of ICI Americas, Inc.

Poly(alkylene-oxide) Triblock Copolymers (Pluronics®)*

Pluronic Type	wt.% PEG block	Average M_n	Prod. No.
PEG-PPG-PEG	82.5	14,600	**542342**
PEG-PPG-PEG	80	8,400	**412325**
PPG-PEG-PPG	50	2,000	**435473**
PEG-PPG-PEG	50	1,900	**435414**
PPG-PEG-PPG	40	2,700	**435481**
PEG-PPG-PEG	40	2,900	**435449**
PEG-PPG-PEG	30	4,400	**435457**

Pluronic Type	wt.% PEG block	Average M_n	Prod. No.
PEG-PPG-PEG	30	5,800	**435465**
PEG-PPG-PEG	15	2,800	**373850**
PPG-PEG-PPG	10	3,300	**435503**
PEG-PPG-PEG	10	1,100	**435406**
PEG-PPG-PEG	10	2,000	**435422**
PEG-PPG-PEG	10	2,800	**435430**

*PEG-PPG-PEG = poly(ethylene glycol)-*b*-poly(propylene glycol)-*b*-poly(ethylene glycol) (Pluronic); PPG-PEG-PPG = poly(propylene glycol)-*b*-poly(ethylene glycol)-*b*-poly(propylene glycol) (Pluronic R). Brij is a registered trademark of ICI Americas, Inc. Pluronic is a registered trademark of BASF AG.

Electrospinning: An Enabling Technique for Nanostructured Materials

Dr. Jingwei Xie and Prof. Younan Xia

Department of Biomedical Engineering,
Washington University, St. Louis, MO

Introduction

Fibrous nanomaterials are attractive for a range of applications due to their intrinsically high porosities and large surface areas. Electrospinning is a simple, versatile technique for generating nanofibers from a rich variety of materials including polymers, composites, and ceramics.[1,2] **Figure 1** shows a typical electrospinning setup that consists of three major components: a high-voltage power supply, a spinneret, and an electrically conductive collector. A hypodermic needle and a piece of aluminum foil serve well as the spinneret and collector, respectively. The liquid (a melt or solution) for electrospinning is loaded into a syringe and fed at a specific rate set by a syringe pump. In some cases, a well-controlled environment (e.g., humidity, temperature, and atmosphere) is critical to the operation of electrospinning, especially for the fabrication of ceramic nanofibers.[3]

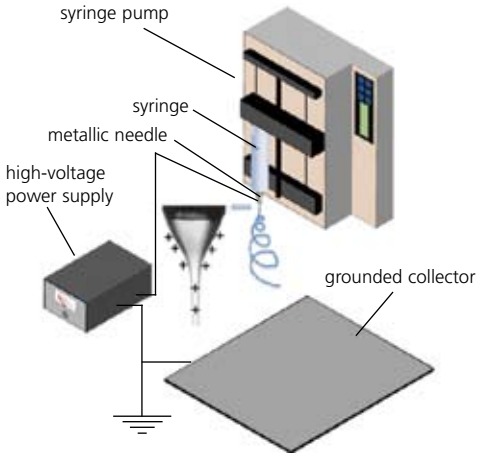

Figure 1. Schematic of a typical setup for electrospinning.

In this article, we discuss issues critical to successful application of the electrospinning technique, including control of individual nanofibers to form secondary structures and assembly of nanofibers into 3D architectures. We illustrate a few of the many potential applications of electrospun nanofibers, especially in the area of vascular grafting and tissue engineering.

Mechanism of Nanofiber Formation

Although the setup for electrospinning is extremely simple, the spinning mechanism is rather complicated. The essence of electrospinning is to generate a continuous jet by immobilizing charges on the surface of a liquid droplet. It has recently been resolved that the spinning process is solely a result of whipping rather than splaying of a liquid jet.[4,5] The whipping instability originates from the electrostatic interactions between the external electric field and the surface charges on the jet. Stretching and acceleration of the unstable fluid filament, where the liquid phase has to maintain an appropriate viscoelasticity in order to survive the whipping process, results in the formation of fibers with nanoscale diameters. Electrospun fibers are typically several orders in magnitude smaller than those produced using conventional spinning techniques. By optimizing parameters such as: *i*) the intrinsic properties of the solution including the polarity and surface tension of the solvent, the molecular weight and conformation of the polymer chain, and the viscosity, elasticity, and electrical conductivity of the solution; and *ii*) the operational conditions such as the strength of electric field, the distance between spinneret and collector, and the feeding rate of the solution, electrospinning is capable of generating fibers as thin as tens of nanometers in diameter.[1]

Controlling Individual Nanofibers

In the early days, electrospinning was mainly used to prepare polymeric nanofibers, and so far it has been successfully applied to more than 100 types of natural and synthetic polymers.[6] Recently, electrospinning was integrated with sol-gel chemistry to generate composite and inorganic nanofibers.[3] Polymers, such as poly(vinyl pyrrolidone) (PVP, **437190**), poly(vinyl alcohol) (PVA, **341584**), or poly(ethylene oxide) (PEO, **189456**) can be processed from solutions containing a sol-gel precursor, followed by selective removal of the organic phase via calcination in air. This approach can be applied to essentially any oxide material with an available sol-gel precursor (e.g., a metal alkoxide). Notable examples include: Al_2O_3, SiO_2, TiO_2, SnO_2, V_2O_5, ZnO, Co_3O_4, Nb_2O_5, MoO_3, GeO_2, ITO, $NiFe_2O_4$, $LiCoO_2$, $MgNiO_2$, and $BaTiO_3$.[7–9] With the use of specially designed precursor polymers such as poly(norbornenyldecaborane), the capability of electrospinning has been further extended to fabricate non-oxide ceramic nanofibers such as silicon carbide and boron carbide.[10] These inorganic nanofibers are expected to find use in applications related to energy conversion, energy storage, and structural reinforcement.

Electrospinning has also been conducted with a spinneret consisting of co-axial or side-by-side capillaries to generate nanofibers with a variety of secondary structures including core-sheath or porous fibers and nanotubes with single or multiple channels.[11–16] **Figure 2a** shows SEM image of TiO_2 (anatase) nanotubes that were fabricated by electrospinning with a co-axial spinneret, followed by calcination in air. In a typical process, the inner and outer capillaries were fed with mineral oil and an alcoholic solution containing PVP and $Ti(O\textit{i}Pr)_4$ (**205273**), respectively. A co-axial jet was formed because the oily and alcoholic phases could not mix during the spinning process. Electrospun fibers can also be made

ALDRICH Chemistry

porous by modifying the collection scheme. For example, we have demonstrated the fabrication of highly porous fibers by electrospinning the jet directly into a cryogenic liquid.[17] Well-defined pores developed on the surface of each fiber as a result of temperature-induced phase separation between the polymer and the solvent and the evaporation of solvent under a freeze-drying condition. **Figure 2b** shows SEM image of porous poly(styrene) fibers prepared using this method. The inset shows a cross-sectional image of a broken fiber, indicating that the fiber was porous throughout. This approach has been extended to a number of polymers including poly(vinylidene fluoride) (**427152**), poly(acrylonitrile) (**181315**), and poly(ε-caprolactone) (**181609**).

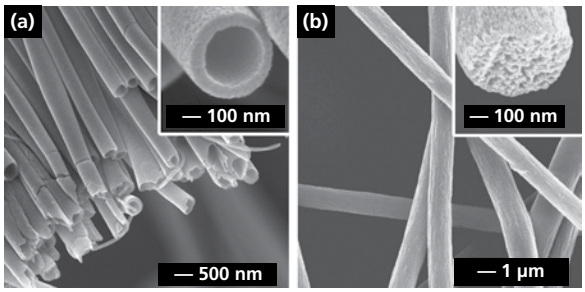

Figure 2. (a) SEM image of a uniaxially aligned array of TiO_2 (anatase) nanotubes. Reprinted from Ref. 13 with permission from American Chemical Society. (b) SEM images of polystyrene porous fibers fabricated by electrospinning the jet into a liquid nitrogen bath, followed by drying in vacuo. Reprinted from Ref. 17 with permission from American Chemical Society.

Controlling the Alignment and Assembly of Nanofibers

Electrospun fibers are usually deposited on the collector as a non-woven mat, in which the fibers take a completely random orientation (see **Figure 3a**). Several approaches have been developed to organize electrospun fibers into aligned arrays. For example, electrospun fibers can be aligned into a uniaxial array by replacing the single-piece collector with a pair of conductive substrates separated by a void gap.[11] In this case, the nanofibers tend to be stretched across the gap oriented perpendicular to the edges of the electrodes. It was also shown that the paired electrodes could be patterned on an insulating substrate such as quartz or polystyrene so the uniaxially aligned fibers could be stacked layer-by-layer into a 3D lattice (see **Figure 3b**). By controlling the electrode pattern and/or the sequence for applying high voltage, it is also possible to generate more complex architectures consisting of well-aligned nanofibers.[12]

Figure 3c shows SEM image of a uniaxial array of carbon nanofibers that were electrospun from a solution of poly(acrylonitrile) in dimethylformamide, followed by stabilization in air and carbonization. This approach can, in principle, be applied to any electrospinable material since the alignment is mainly determined by the arrangement of electrodes in the collector. **Figure 3d** shows SEM image of a tri-layered thin film of poly(vinyl pyrrolidone) nanofibers that were deposited across three pairs of electrodes by alternately connecting each pair to the high voltage supply. The nanofibers in each layer were uniaxially aligned, with their long axes rotated by 60 degrees between adjacent layers. Uniaxially aligned nanofibers between two fixed points could also be twisted to form bundles and other types of constructs (e.g., a micrometer-sized yarn by braiding three nanofiber bundles manually).[18] In related work, the continuous yarns consisting of aligned nanofibers were further woven into textiles for various applications.[19]

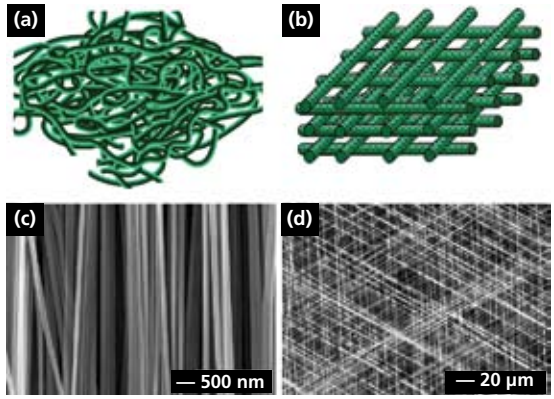

Figure 3. (a) Schematic of nanofibers with random orientation. (b) Schematic of a 3D lattice of nanofibers. (c) SEM image of a uniaxially aligned array of carbon nanofibers. Reprinted from Ref. 11 with permission from American Chemical Society. (d) SEM image of a layer-by-layer stacked thin film of PVP nanofibers. Reprinted from Ref. 12 with permission from Wiley-VCH.

Electrospun nanofibers could also be directly deposited on various objects to obtain nanofiber-based constructs with well-defined and controllable shapes. **Figure 4a** shows the side view of a poly(propylene carbonate) (PPC, **389021**) tube (2 mm in diameter) fabricated by depositing electrospun fibers onto a cylindrical rod, followed by removal of the rod.[20] The inset shows a cross-sectional view of the tube. In addition, one can manually process membranes of aligned or randomly oriented nanofibers into various types of constructs after electrospinning: for example, fabrication of a tube by rolling up a fiber membrane or the preparation of discs with controllable diameters by punching a fiber membrane. **Figure 4b** shows the cross-sectional view of a nerve conduit made of aligned fibers containing glial cell line-derived neurotrophic factor (GDNF, **G1401**).[21] The conduit was simply fabricated by rolling up the fiber membrane and suturing the connection site with dichloromethane. More work remains to be done in the future in order to organize electrospun nanofibers into the 3D architectures desirable for a range of applications.

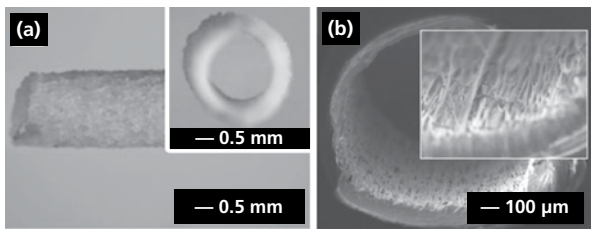

Figure 4. (a) Side and cross-sectional (inset) view of an electrospun PPC tube. Reprinted from Ref. 20 with permission from Blackwell Publishing. (b) Cross-sectional view of a nerve conduit with aligned GDNF-encapsulated fibers. Reprinted from Ref. 21 with permission from Wiley-VCH.

Application in Tissue Engineering

Electrospun nanofibers offer great promise for engineering of artificial skins, muscles, blood vessels (vascular grafts), orthopedic components (bones, cartilages, and ligaments/tendon), and peripheral/central nervous system components. Non-woven mats of electrospun nanofibers can serve as ideal scaffolds for tissue engineering because they can mimic the extracellular matrices (ECM) in that the architecture of nanofibers is similar to the collagen structure of the ECM – a 3D network of collagen nanofibers 50–500 nm in diameter. Furthermore, electrospun nanofibers have several advantages for tissue regeneration: correct topography (e.g., 3D porosity, nanoscale size, and alignment), encapsulation and local sustained release of growth factors, and surface functionalization (e.g., attachment of functional groups). Materials used for tissue engineering must be biocompatible and notable examples include natural or synthetic biodegradable polymers, biocompatible polymers, and blends with bioactive inorganic materials (e.g. hydroxyapatite **574791**).

Electrospun fibers can be used to fabricate artificial blood vessels. Aligned nanofibers of biodegradable poly(L-lactide-*co*-ε-caprolactone) (**457639**) have been evaluated as a potential scaffold for blood vessel engineering through culturing human coronary artery smooth muscle cells.[22] In another study, the composition and mechanical properties of a vascular graft scaffold fabricated from blends of Type-I collagen (**C3511**), elastin, and poly(D, L-lactide-*co*-glycolide) (**531154**) were found to be similar to those of native blood vessels and the grafts were biocompatible and did not induce local or systemic toxic effects when implanted *in vivo*.[23] One remaining problem is to achieve sufficient cellular infiltration into the electrospun fibrous matrix. This was partially solved by combining electrospinning and electrospraying to fabricate cell-microintegrated blood vessel constructs — conduits that were highly cellularized with smooth muscle cells (SMCs) in the interior of the walls.[24] These conduits were shown to be cytocompatible, strong, and possess compliance values similar to native blood vessels.

Electrospun fibrous scaffolds can be combined with gene therapy and stem cell biology to provide a new route to blood vessel regeneration. For example, a vascular graft has been fabricated by seeding genetically modified autologous mesenchymal stem cell (MSCs) onto a tubular scaffold of electrospun poly(propylene carbonate) and the seeded cells could then be integrated into the microstructure of the graft to form a 3D cellular network.[25] In another work, bone marrow MSCs in poly(L-lactic) acid (PLLA, **38534**) nanofibrous vascular grafts have been demonstrated to be antithrombogenic *in vivo*.[26] **Figure 5a** and **5b** show confocal micrographs of the human aortic SMCs and bone marrow MSCs seeded on aligned PLLA nanofibers surface. It can be clearly seen that the cellular organization and alignment were similar to that of the native artery. In this study, the aligned PLLA nanofibers were fabricated as a membrane by electrospinning and then rolled up into a tubular graft with the incorporation of marrow MSCs (see **Figure 5c**). **Figure 5d** shows a photograph where the vascular graft composed of PLLA nanofibers and MSCs was sutured to the common carotid artery (CCA) of a rat. These results demonstrated that nanofibrous scaffolds allowed the remodeling of vascular grafts in both cellular and ECM contents, similar to that of the native artery.

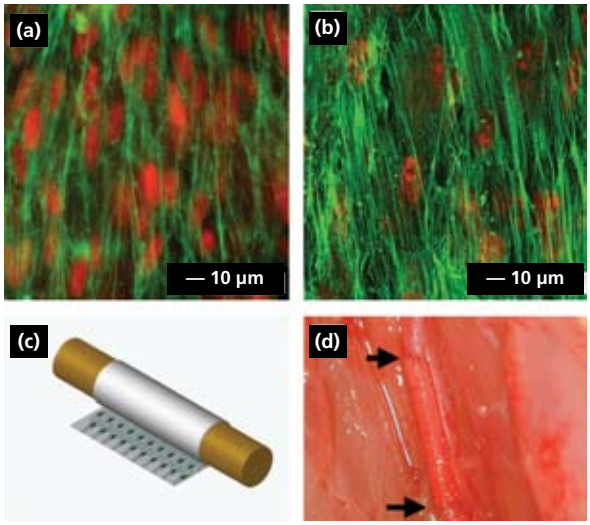

Figure 5. (a, b) Human aortic smooth muscle cells and bone marrow stem cells seeded on thin films of aligned PLLA nanofibers. The actin filaments were stained with FITC-conjugated phalloidin (green), and the nuclei were counterstained using propidium iodide (red). (c) The tubular graft formed by rolling the cell-embedded fibrous membrane. (d) An end-to-end view of the vascular graft sutured to the common carotid artery in a rat. Reprinted from Ref. 26 with permission from the National Academy of Sciences of the USA.

Conclusion

The past five years have witnessed tremendous progress in the area of electrospinning. The capabilities of many well-established techniques for material processing can be greatly enhanced by combining them with electrospinning. The composition, morphology, and structures of fibers could be further tailored using a number of physical and/or chemical methods. For example, encapsulation has been exploited to provide a simple route to multifunctional nanofibers.[27,28] All of these research activities have led to the exploitation of electrospun nanofibers in a broad range of applications. It is expected that research on this technique will become more interdisciplinary in the future. With the involvement of a larger scientific and engineering community, electrospinning will surely become one of the most powerful tools for fabricating nanostructured materials with the broadest range of functionalities and applications.

References

(1) Li, D.; Xia, Y. *Adv. Mater.*, **2004**, *16*, 1151. (2) Dzenis, Y. *Science*, **2004**, *304*, 1917. (3) Li, D.; McCann, J. T.; Xia, Y. *J. Am. Ceram. Soc.*, **2006**, *89*, 1861. (4) Hohman, M. M.; Shin, M.; Rutledge, G. C.; Brenner M. P. *Phys. Fluids*, **2001**, *13*, 2201. (5) Hohman, M. M.; Shin, M.; Rutledge, G. C.; Brenner, M. P. *Phys. Fluids*, **2001**, *13*, 2221. (6) Burger, C.; Hsiao, B. S.; Chu, B. *Ann. Rev. Mater. Res.*, **2006**, *36*, 333. (7) Li, D.; Xia, Y. *Nano. Lett.*, **2003**, *3*, 555. (8) McCann, J. T.; Chen, J. I. L.; Li, D.; Ye, Z.; Xia, Y. *Chem. Phys. Lett.*, **2006**, *424*, 162. (9) Larson, G.; Velarde-Ortiz, R.; Minchow, K.; Barrero, A.; Loscertales, I. G. *J. Am. Chem. Soc.*, **2003**, *125*, 1154. (10) Welna, D. T.; Bender, J. D.; Wei, X.; Sneddon, L. G.; Allcock, H. R. *Adv. Mater.*, **2005**, *17*, 859. (11) Li, D.; Wang, Y.; Xia, Y. *Nano. Lett.*, **2003**, *3*, 1167. (12) Li, D.; Wang, Y.; Xia, Y. *Adv. Mater.*, **2004**, *16*, 361. (13) Li, D.; Xia, Y. *Nano. Lett.*, **2004**, *4*, 933. (14) Liu, Z.; Sun, D.; Guo, P.; Leckie, J. *Nano. Lett.*, **2007**, *11*, 1081. (15) Zhao, Y.; Cao, X.; Jiang, L. *J. Am. Chem. Soc.*, **2007**, *129*, 764. (16) Li, D.; McCann, J. T.; Xia, Y. *Small*, **2005**, *1*, 83. (17) McCann, J. T.; Marquez, M.; Xia, Y. *J. Am. Chem. Soc.*, **2006**, *128*, 1436. (18) Teo, W. E.; Ramakrishna, S. *Nanotechnology*, **2005**, *16*, 1878. (19) Smit, E.; Buttner, U.; Sanderson, R. D. *Polym Commun.*, **2005**, *46*, 2419. (20) Zhang, J.; Qi, H.; Wang, H.; Hu, P.; Ou, L.; Guo, S.; Li, J.; Che, Y.; Yu, Y.; Kong, D. *Artificial Organs*, **2006**, *30*, 898. (21) Chew, S. Y.; Mi, R.; Hoke, A.; Leong, K.W. *Adv. Funct. Mater.*, **2007**, *17*, 1288.

ALDRICH Chemistry

(22) McCann, J. T.; Marquez, M.; Xia, Y. *Nano. Lett.*, **2006**, *6*, 2868. (23) Xu, C. Y.; Inai, R.; Kotaki, M.; Ramakrishna, S. *Biomaterials*, **2004**, *25*, 877. (24) Stitzel, J.; Liu, J.; Lee, S. J.; Komura, M.; Berry, J.; Soker, S.; Lim, G.; Dyke, M. V.; Czerw, R.; Yoo, J. J.; Atala, A. *Biomaterials*, **2006**, *27*, 1088. (25) Stankus, J. J.; Soletti, L.; Fujimoto, K.; Hong, Y.; Vorp, D. A.; Wagner, W. R. *Biomaterials*, **2007**, *28*, 2738. (26) Hashi, C. K.; Zhu, Y.; Yang, G. Y.; Young, W. L.; Hsiao, B. S.; Wang, K.; Chu, B.; Li, S. *PNAS*, **2007**, *104*, 11915. (27) Wang, A.; Singh, H.; Hatton, T. A.; Rutledge, G. C. *Polymer*, **2004**, *45*, 5505. (28) Lu, X. F.; Zhao, Y. Y.; Wang, C. *Adv. Mater.*, **2005**, *17*, 24.

Polymers for Electrospinning

The following is a selection of polymers successfully used for electrospinning into nanoscale fibers. While higher molecular weight polymers are frequently used for electrospinning, polymers with lower molecular weight and even small molecules (e.g. lecithin **P2394**) can be processed from cross-linked or gelled solutions.

For a complete list of synthetic polymers, visit ***sigma-aldrich.com/polymer***.
For a complete list of biodegradable and natural polymers, visit ***sigma-aldrich.com/biomaterials***.

Synthetic Polymers

Nylon 6

Polycaprolactam
[*25038-54-4*]

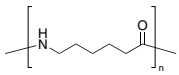

181110-25G	25 g
181110-500G	500 g
181110-1KG	1 kg

Polyacrylonitrile

PAN
[*25014-41-9*]

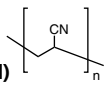

▸ **average M_w ~150,000 (Typical)**

181315-50G	50 g
181315-100G	100 g

Poly(ethylene oxide)

PEO
[*25322-68-3*]

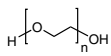

▸ **average M_w ~100,000**

181986-5G	5 g
181986-250G	250 g
181986-500G	500 g

▸ **average M_w ~600,000**

182028-5G	5 g
182028-250G	250 g
182028-500G	500 g

▸ **average M_w ~1,000,000**

372781-5G	5 g
372781-250G	250 g
372781-500G	500 g

Poly(methyl methacrylate)

PMMA
[*9011-14-7*]

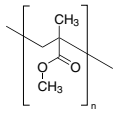

▸ **M_w ~120,000 by GPC**

182230-25G	25 g
182230-500G	500 g
182230-1KG	1 kg

Polystyrene

PS
[*9003-53-6*]

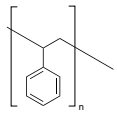

▸ **average M_w ~350,000**

441147-1KG	1 kg
441147-3KG	3 kg

Poly(propylene carbonate)

PPC
[*25511-85-7*]

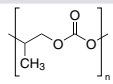

▸ **average M_w ~50,000 by GPC**

389021-25G	25 g
389021-100G	100 g

Poly(vinyl acetate)

PVA, PVAc
[*9003-20-7*]

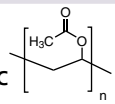

▸ **average M_w ~113,000 by GPC**

189480-25G	25 g
189480-500G	500 g
189480-1KG	1 kg

▸ **average M_w ~500,000 by GPC**

387932-500G	500 g

Poly(ethylene-*co*-vinyl acetate), vinyl acetate: 40 wt.%

[*24937-78-8*]

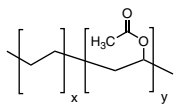

▸ **Melt index (190 °C /2.16kg) 57 g/10 min**

340502-250G	250 g

Poly(vinyl alcohol), 99+% hydrolyzed

PVOH, PVA
[*9002-89-5*]

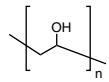

▸ **average M_w 89,000-98,000**

341584-25G	25 g
341584-500G	500 g
341584-1KG	1 kg

Polyvinylpyrrolidone

PVP
[*9003-39-8*]

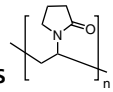

▸ **average M_w ~1,300,000 by LS**

437190-25G	25 g
437190-500G	500 g
437190-1KG	1 kg

Poly(vinylidene fluoride)

PVDF
[*24937-79-9*]

▸ **average M_w ~180,000 by GPC**

427152-100G	100 g
427152-250G	250 g

Poly(vinylidene fluoride-*co*-hexafluoro-propylene)

[*9011-17-0*]

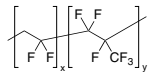

▸ **average M_w ~400,000 (bimodal distribution)**

427160-100G	100 g
427160-250G	250 g

Polycarbomethylsilane

Polycarbosilane
[*62306-27-8*]
Polymeric precursor for SiC ceramics

▸ **average M_w ~800, electronic grade**

522589-25G	25 g

Biodegradable Polymers

Poly-(L-lactide)

L-PLA, PLLA
[*33135-50-1*]

▸ **average M_w ~100,000–150,000**

531170-1G	1 g
531170-5G	5 g

Poly(DL-lactide)

DL-PLA, PDLLA
[*51063-13-9*]

▸ **average M_w ~75,000–120,000**

531162-1G	1 g
531162-5G	5 g

Poly(DL-lactide-*co*-glycolide) (50:50)

PLGA
[*26780-50-7*]

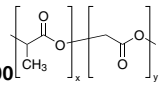

▸ **average M_w 5,000-15,000**

531154-1G	1 g
531154-5G	5 g

▸ **average Mw ~ 40,000-75,000**

P2191-1G	1 g
P2191-5G	5 g

Poly(DL-lactide-*co*-caprolactone)

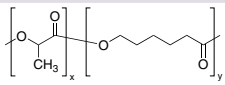

▸ **x:y=86:14**

457647-1G	1 g
457647-5G	5 g

▸ **x:y=40:60**

457639-1G	1 g
457639-5G	5 g

Polycaprolactone

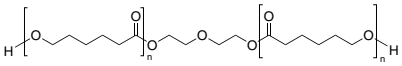

PCL
[*24980-41-4*]

▸ **average M_w ~10,000 by GPC**

440752-5G	5 g
440752-250G	250 g
440752-500G	500 g

▸ **average M_w ~80,000 by GPC**

440744-5G	5 g
440744-250G	250 g
440744-500G	500 g

Natural Polymers

Cellulose acetate, 39.7 wt.% acetyl

[*9004-35-7*]

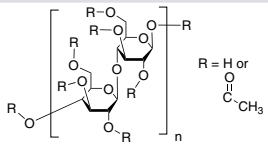

▸ **average M_n ~50,000 by GPC**

419028-25G	25 g
419028-500G	500 g

Poly(3-hydroxybutyric acid)

polyhydroxybutyrate, PHB
[*29435-48-1*]

▸ **natural origin**

363502-10G	10 g
363502-100G	100 g

Poly(3-hydroxybutyric acid-*co*-3-hydroxyvaleric acid)

PHB-*co*-PHV
[*80181-31-3*]

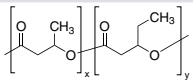

▸ **produced via a controlled fermentation process using microorganisms**

▸ **12 wt.% PHV**

403121-10G	10 g
403121-100G	100 g

▸ **8 wt.% PHV**

403113-10G	10 g
403113-100G	100 g

▸ **5 wt.% PHV**

403105-10G	10 g
403105-100G	100 g

Collagen from calf skin, Type III

[*9007-34-5*]

C3511-10MG	10 mg
C3511-50MG	50 mg
C3511-100MG	100 mg
C3511-250MG	250 mg
C3511-1G	1 g

Chitosan

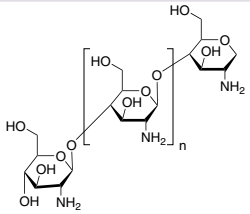

Poly(D-glucosamine)
[*9012-76-4*]

▸ **Low molecular weight**

448869-50G	50 g
448869-250G	250 g

▸ **Medium molecular weight**

448877-50G	50 g
448877-250G	250 g

▸ **High molecular weight**

419419-50G	50 g
419419-250G	250 g

Gelatin from bovine skin, Type B

[*9000-70-8*]

▸ **average Mw ~ 50,000 (~ 225 Bloom)**

G9382-100G	100 g
G9382-500G	500 g
G9382-1KG	1 kg

Fibrinogen, Fraction I, type I: From Human Plasma

Factor I
[*9001-32-5*]

▸ **Soluble dimer Mw ~ 340,000**

F3879-100MG	100 mg
F3879-250MG	250 mg
F3879-1G	1 g
F3879-5G	5 g

Elastin, soluble bovine

[*9007-58-3*]

▸ **from neck ligament**

E6527-1G	1 g

Commercial Volumes of Quantum Dots: Controlled Nanoscale Synthesis and Micron-Scale Applications.



Drs. Nigel L. Pickett, Ombretta Masala, James Harris

Nanoco Technologies, Ltd., Manchester, United Kingdom

Introduction

Quantum dots (QDs) are luminescent semiconductor nanoparticles, with diameters in the range of 1 to 20 nm. The unique optical and electronic properties of QDs are being exploited in a number of applications including flat panel displays and coloured lighting along with fluorescent imaging in biological and medical diagnostics. It is envisaged that QDs may replace many of the existing organic dyes and inorganic phosphors currently used in imaging, display and lighting devices.

Quantum confinement of electrons in semiconductor crystals with well-defined 3-dimensional nanoscale size is the origin of unique QD properties compared to conventional materials.[1–4] Fundamentally, the quantum confinement effect results in an increasing semiconductor bandgap with decreasing QD size. This allows size-dependent tuning of the semiconductor photoluminescence emission wavelength throughout the visible spectrum. Combined with a very sharp emission spectrum and high quantum efficiency, it makes QDs ideal luminophors for many optoelectronics and imaging applications. Just as the synthesis of high quality macroscale semiconductors has facilitated the development of optoelectronics over 5 decades ago, nanoscale control of semiconductor architecture to make QD nanoparticles can enable future technologies, including high-efficiency solar cells, solid-state light sources, and ultra-bright displays.

Nanocrystals are often described as "artificial atoms." Like atoms, electron energy levels of nanocrystals are discrete but the fundamental difference is that the level spacing and other quantum mechanical properties can be tailored by adjusting the nanocrystal size. If we consider a nanocrystal like an artificial atom, then it should be possible to combine them into "nanocrystal molecules" and "nanocrystal solids" or, more generally, into nanocrystal assemblies in the same way as observed with real atoms. Therefore QD nanocrystals can be considered as building blocks of new solid-state materials and devices with novel physical properties. Building upon the development of synthetic routes to high quality QDs and a rigorous understanding of the physical properties of individual QDs, it is possible to control and manipulate QD assemblies and open up routes to fabrication of novel devices with enhanced physical, optical and electronic properties.

High-quality QDs: Shelling and Organic Passivation

Quantum confinement effects exist in many nm-scale semiconductor structures. However, simply reducing size of semiconductor colloids down to nm-scale is insufficient for making high-quality QDs for demanding commercial applications. Important metrics for describing QDs useful in applications are: 1) fluorescence quantum yield (QY), defined as the ratio of the number of photons emitted to the number of photons absorbed reported as a percentage; 2) narrow particle size distribution below +/- 5%; 3) sharp emission peak widths defined by their full width half max (FWHM), that is, the width of the peak half way up the emission spectrum.

QDs have surface atoms with available coordination sites that render them highly reactive and susceptible to particle agglomeration. To overcome this problem QDs are passivated by capping the surface atoms with protecting groups. Capping the QDs serves four purposes: 1) it prevents particle agglomeration, 2) protects the particle from the surrounding chemical environment, 3) provides additional electronic stabilization to the surface, and 4) controls solubility in a specific solvent system. The capping agent usually takes the form of a Lewis base covalently bound to surface metal atoms. Other capping agents such as an organic polymer forming a sheath around the particle have also been employed to enhance particle stability.

Simple semiconductor colloids consisting of a crystalline core and an outer organic passivating layer can have relatively low QY due to electron-hole recombination occurring at defects and dangling bonds situated on the nanocrystal surface. Building up complex 3-dimensional nanocrystal architectures can substantially enhance size-dependent luminescence of core semiconductor nanoparticles. Growing a second, wider bandgap inorganic material over the core will eliminate core surface defects and dangling bonds. The resulting core/shell QDs have greatly improved QY. An alternative strategy employed by Nanoco is to prepare a core/multi-shell structure where the electron-hole pair is completely confined to a single shell layer.[5] This is known as a quantum dot-quantum well (QDQW) structure, and consists of a wide bandgap core, followed by a thin layer (1–5 monolayers) of a narrower bandgap material which is then surrounded by another wide bandgap material, e.g. ZnS/CdSe/ZnS. These QDQWs exhibit clear confinement of photo-excited carriers in the CdSe layer and the emission wavelength can be tuned by changing the thickness of the CdSe shell. The QDQW methodology is especially useful for making high quality blue-emitting QDs with improved optical and chemical stability. Schematics of core, core/shell and core/multi-shell QDs are described in **Figure 1**. By making reproducible core-shell and core/multi-shell nanocrystals, Nanoco is able to provide QDs with exceptional stability and very high QY, required in a variety of technological applications.[5]

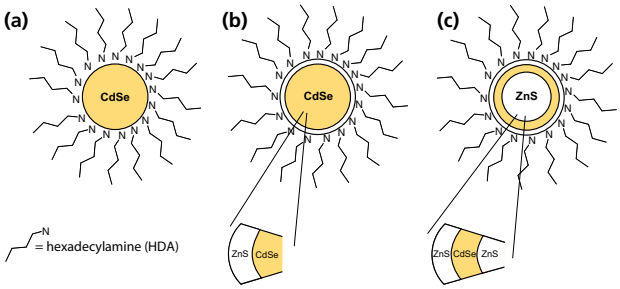

Figure 1. 3D architectures of QDs: (a) A core particle consisting of a CdSe core and HDA organic capping agent. (b) A core-shell particle consisting of a CdSe core, a ZnS shell, and HDA capping agent. (c) A core-multi shell (QDQW) particle consisting of a ZnS core and a CdSe shell followed by a ZnS shell with HDA capping agent.

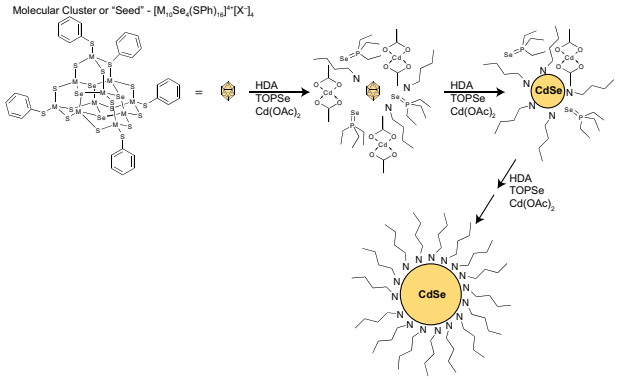

Figure 2. Molecular seeding synthesis of a cadmium selenide quantum dot using $[M_{10}Se_4(SPh)_{16}][x]_4$ x = Li^+ or $(CH_3)_3NH^+$ as the molecular seed and dropwise addition of cadmium acetate ($Cd(OAc)_2$) and tri-n-octylphosphine selenide (TOPSe) as the cadmium and selenium element-source precursors, with hexadecylamine (HDA) used as the capping agent.

Enabling applications — Scaling up QD production

To make QDs useful for lighting and display applications, synthetic routes are needed to reproducibly yield pure, high-quality, monodispersed crystalline QDs. These synthetic methods must be scalable. For example, for use as a down conversion phosphor, milligram quantities are needed per LED but, because millions of LEDs are fabricated monthly, synthetic methods capable of delivering multi-kilogram quantities are required. To do this, Nanoco developed "molecular seeding" methods.[6–8]

Until recently, the main method employed to prepare semiconductor QDs was classical colloid chemistry of controlled or arrested nanocrystal precipitation from precursor solutions. Typically, separate elemental precursors needed to form a compound semiconductor were rapidly injected into a reaction flask to achieve rapid homogeneous nucleation of semiconductor nanocrystals. These "dual injection" methods work well for small-scale synthesis where one solution can be added rapidly to another while maintaining a constant temperature throughout the reaction. With increasing reaction scales rapid injection of large solution volumes into one another results in temperature differentials and culminates in wide particle size distributions. Nanoco Technologies' molecular seeding methodology has been developed to enable reproducible routes to larger quantities of crystalline, narrow size-dispersity, stable QDs. In the presence of a molecular cluster compound and chemical precursors, QDs are produced under conditions whereby the integrity of the molecular cluster is maintained and acts as a prefabricated seed template. A schematic of the molecular seeding methodology is described in **Figure 2**. Individual molecules of a cluster compound act as seeds or nucleation points upon which nanoparticle growth can be initiated. Consequently, because suitable nucleation sites are already provided in the system by the molecular clusters, a high temperature nucleation step is not necessary to initiate nanoparticle growth and the methodology is scalable. Nanoco has demonstrated that each individual molecular cluster does indeed end up as a QD.[9]

Future: CFQDs-Cadmium Free Quantum Dots

The use of cadmium and other restricted heavy metals in semiconductor QDs is a major concern for commercial applications. In many regions of the world there is now, or soon will be, legislation to restrict and, in some cases, ban the use of materials containing heavy metals including Cd, Hg, and Pb.[10] Nanoco's molecular seeding method has been adapted for other compound semiconductor materials (e.g. III-V's), which have similar optical properties to those of CdSe QDs, but do not contain heavy metals. Over the coming months, Nanoco plans to provide small samples of these materials for commercial sale through Sigma-Aldrich®.

Case Study Quantum Dot Solid State Lighting (QD-SSL)

The white light LED market is hugely important, with the promise of increased lamp lifetimes and efficiencies paving the way for a revolution in the lighting industry. Color rendering and efficiency are the two most important criteria for traditional light sources for general lighting. Lamp color is typically specified according to the CIE 1931 chromaticity diagram (**Figure 3**). The ability of a light source to illuminate an object's true color is denoted by its color rendering index. For example, sodium lamp street lighting has poor color rendering capability as it's difficult to distinguish a red car from a yellow car.

Current white light LED technology utilizes a cerium doped YAG:Ce (yttrium aluminium garnet) down-conversion phosphor pumped by a blue (450 nm) LED chip. The combination of blue light from the LED and a broad yellow emission from the YAG phosphor results in white light. Unfortunately, this white light often appears somewhat blue and is often described as "cold" or "cool" white. QDs can be used as LED down-conversion phosphors because they exhibit a broad excitation spectrum and high quantum efficiencies. Furthermore, the wavelength of the emission can be tuned completely across the visible region simply by varying the size of the dot or the type of semiconductor material. As such, they have the potential to be used to generate virtually any color and, more importantly, warm whites strongly desired by the lighting industry. Additionally, by using a combination of one to three different types of

ALDRICH Chemistry

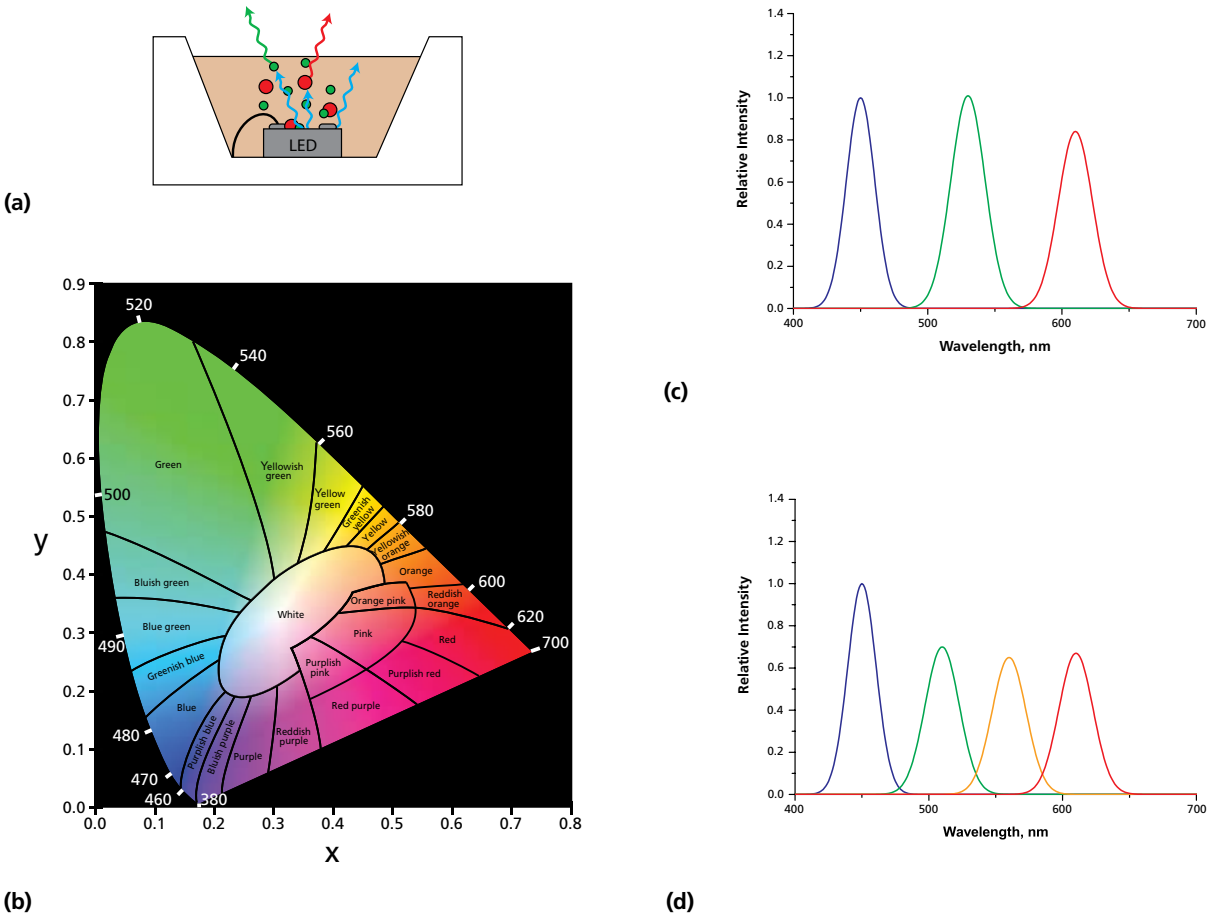

Figure 3. (a) Schematic of quantum dot LED: QDs are optically pumped by a visible blue GaN LED to produce green and red photoluminescence. The mixture of red, green and blue produces a white light. (b) CIE 1931 chromaticity diagram: A mixture of two colors produces a new color whose xy coordinate falls on the line connecting their respective xy coordinates. A mixture of three colors produces new color whose xy coordinate falls within a triangle whose vertices correspond to the xy coordinates of the three independent colors. The location of the coordinates of the mixed color will depend on the relative intensities of the source colors. (c) Spectrum of a trichromatic-dual QD LED utilizing blue LED chip with green and red QDs. (d) Spectrum of a quadchromatic-triple QD LED blue LED chip; green, yellow and red QDs. Note: both spectra have 1931 CIE x,y coordinates of 0.311, 0.324 but the color rendering index increases from c to d.

dots with emission wavelengths corresponding to green, yellow, and red it is possible to achieve white lights of different color rendering indexes (Figure 3). Because of these attractive features, QD-LEDs are beginning to receive attention from both industrial and academic researchers.[11–15]

In addition to white lighting for general illumination, there are other opportunities for QD-LEDs. For example, green LEDs are not particularly efficient, thus green-emitting QDs on top of an efficient blue LED chip may be a solution. Similarly, amber LEDs suffer from temperature dependencies and thus a QD solution may be applicable. Furthermore, because of the widely tunable QD emission, it's possible to have near UV-pumped QD-LEDs with combinations of QDs which emit virtually any color on the chromaticity diagram. This could have important applications in signage by, for example, replacing neon bulbs.

References

(1) Guyout-Sionest, P. *Material Matters*, **2007**, *2*, *1* 10. (2) Semiconductor Nanoclusters – Physical, Chemical, and Catalytic Aspects; Kamat, P. V.; Meisel, D., Eds.; Studies in Surface Science and Catalysis; Elsevier: Amsterdam, 2006, 103. (3) Weller, H. *Angew. Chem. Int. Ed. Engl*, **1993**, *32*, 41. (4) Weller, H. *Adv. Mater.*, **1993**, *5*, 88. (5) Pickett, N.L.; Daniels, S.; O'Brien; P Patent PCT/GB2006/003028, 2006 (6) Pickett, N.L.; Daniels, S.; O'Brien; P Patent PCT/GB2005/001611, 2005. (7) Pickett, N.L.; Daniels, S.; Patent PCT/GB2006/004003, 2006. (8) Pickett, N.L.; Daniels, S.; Mushtaq, I.; Patent UK/GB2007/0714865.3. 2007. (9) Pickett, N.L.; Masala, O.; Daniels, S.; O'Brien, P.; Helliwell, M. unpublished results. (10) Beginning 1 July 2006, the European Union (EU) directive 2002/95/EC, known as the "Restrictions on the use of Hazardous Substances in electronic equipment" (or RoHS), bans the sale of new electrical and electronic equipment containing more than agreed levels of lead, cadmium, mercury, hexavalent chromium, polybrominated biphenyl (PBB) and polybrominated diphenyl ether (PBDE) flame retardants. This law requires manufacturers to find alternative materials and develop new engineering processes for the creation of common electronic equipment. In addition, beginning 1 June 2007, a new European Community Regulation on chemicals and their safe use (EC 1907/2006) known as REACH, deals with the **R**egistration, **E**valuation, **A**uthorisation and Restriction of **C**hemical substances initiates. The REACH Regulation gives greater responsibility to industry to manage the risks from chemicals and to provide safety information on the substances. (11) Chen, H.-S.; Hsu, C.-K.; Hong, H.-Y. *IEEE Photonics Tech. Lett.*, **2006**, *18*, 193. (12) Nizamoglu, S.; Ozel, T.; Sari, E.; Demir, H.V. *Nanotechnology*, **2007**, *18*, 065709. (13) Song, H.; Lee, S. *Nanotechnology*, **2007**, *18*, 255202. (14) Ali, M.; Chattopadhyay, S.; Kumar, A.; Sapra, S.; Chakraborty, S.; Sarma, D.D. *Nanotechnology*, **2007**, *18*, 075401. (15) Nizamoglu, S.; Demir, H.V. *J. Opt. A: Pure Appl. Opt.*, **2007**, *9*, S419.

TO ORDER: Contact your local Sigma-Aldrich office (see back cover), or visit sigma-aldrich.com/matsci.

Illuminate Your Research with Core-Shell Lumidots™

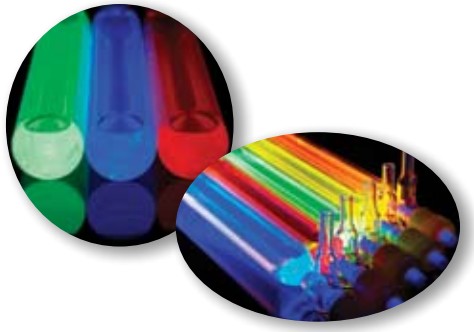

NEW! Core-shell fluorescent quantum dots with emission maxima spanning the entire visible spectrum.

Quantum dots are nanoscale colloidal semiconductors with bandgaps tunable by the size of the colloid. Manufactured by Nanoco Technologies Ltd., the new core-shell Lumidots™ have narrow size distributions and superb fluorescence characteristics. Lumidots are an ideal luminophor for your cutting-edge research, including opto-electronics, anti-counterfeit protection, next-generation solar cells, and biological imaging.

- **Narrow size distribution**
- **Bright, narrow emission (Quantum Yield 30–50%, FWHM < 40 nm)**
- **Core-shell structure for improved stability in applications**
- **Supplied as convenient 2 mL and 10 mL solutions 5 mg/mL in toluene**

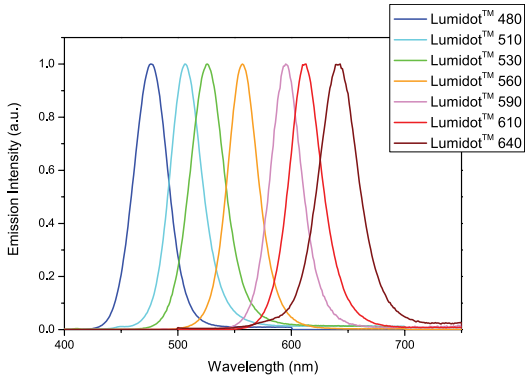

Core-Shell Quantum Dots

For a complete list of quantum dots, including latest products, visit ***sigma-aldrich.com/lumidots***.

Name*	Emission Color	Emission Peak (+/- 5 nm)	FWHM (nm)	Quantity Yield (%)	Extinction Coefficient (10^5 $cm^{-1}M^{-1}$)	Capping Agent**	Prod. No.
Lumidot™ CdSe/ZnS 480	Blue	480	< 40	30–50	0.020	HDA	694592-2ML
							694592-10ML
Lumidot™ CdSe/ZnS 510	Pale Green	510	< 40	30-50	0.045	HDA	694657-2ML
							694657-10ML
Lumidot™ CdSe/ZnS 530	Green	530	< 40	30–50	0.065	HDA	694649-2ML
							694649-10ML
Lumidot™ CdSe/ZnS 560	Yellow	560	< 40	30–50	0.970	HDA	694630-2ML
							694630-10ML
Lumidot™ CdSe/ZnS 590	Orange	590	< 40	30–50	1.60	HDA	694622-2ML
							694622-10ML
Lumidot™ CdSe/ZnS 610	Red	610	< 40	30–50	4.90	HDA	694614-2ML
							694614-10ML
Lumidot™ CdSe/ZnS 640	Deep Red	640	< 60	30–50	5.90	HDA/TOPO	694606-2ML
							694606-10ML

*Supplied as 5 mg/ml solutions in toluene. Product of Nanoco Technologies Ltd: www.nanocotechnologies.com.

**HDA = hexadecylamine, TOPO = trioctylphosphine oxide.

Lumidot is a trademark of Sigma-Aldrich® Biotechnology, LP and Sigma-Aldrich Corp.

Argentina
SIGMA-ALDRICH DE ARGENTINA S.A.
Free Tel: 0810 888 7446
Tel: (+54) 11 4556 1472
Fax: (+54) 11 4552 1698

Australia
SIGMA-ALDRICH PTY LTD.
Free Tel: 1800 800 097
Free Fax: 1800 800 096
Tel: (+61) 2 9841 0555
Fax: (+61) 2 9841 0500

Austria
SIGMA-ALDRICH HANDELS GmbH
Tel: (+43) 1 605 81 10
Fax: (+43) 1 605 81 20

Belgium
SIGMA-ALDRICH NV/SA.
Free Tel: 0800 14747
Free Fax: 0800 14745
Tel: (+32) 3 899 13 01
Fax: (+32) 3 899 13 11

Brazil
SIGMA-ALDRICH BRASIL LTDA.
Free Tel: 0800 701 7425
Tel: (+55) 11 3732 3100
Fax: (+55) 11 5522 9895

Canada
SIGMA-ALDRICH CANADA LTD.
Free Tel: 1800 565 1400
Free Fax: 1800 265 3858
Tel: (+1) 905 829 9500
Fax: (+1) 905 829 9292

China
SIGMA-ALDRICH (SHANGHAI)
TRADING CO. LTD.
Free Tel: 800 819 3336
Tel: (+86) 21 6141 5566
Fax: (+86) 21 6141 5567

Czech Republic
SIGMA-ALDRICH spol. s r. o.
Tel: (+420) 246 003 200
Fax: (+420) 246 003 291

Denmark
SIGMA-ALDRICH DENMARK A/S
Tel: (+45) 43 56 59 10
Fax: (+45) 43 56 59 05

Finland
SIGMA-ALDRICH FINLAND OY
Tel: (+358) 9 350 9250
Fax: (+358) 9 350 92555

France
SIGMA-ALDRICH CHIMIE S.à.r.l.
Free Tel: 0800 211 408
Free Fax: 0800 031 052
Tel: (+33) 474 82 28 00
Fax: (+33) 474 95 68 08

Germany
SIGMA-ALDRICH CHEMIE GmbH
Free Tel: 0800 51 55 000
Free Fax: 0800 64 90 000
Tel: (+49) 89 6513 0
Fax: (+49) 89 6513 1160

Greece
SIGMA-ALDRICH (O.M.) LTD.
Tel: (+30) 210 994 8010
Fax: (+30) 210 994 3831

Hungary
SIGMA-ALDRICH Kft
Ingyenes zöld telefon: 06 80 355 355
Ingyenes zöld fax: 06 80 344 344
Tel: (+36) 1 235 9055
Fax: (+36) 1 235 9050

India
SIGMA-ALDRICH CHEMICALS
PRIVATE LIMITED
Telephone
Bangalore: (+91) 80 6621 9600
New Delhi: (+91) 11 4165 4255
Mumbai: (+91) 22 2570 2364
Hyderabad: (+91) 40 4015 5488
Fax
Bangalore: (+91) 80 6621 9650
New Delhi: (+91) 11 4165 4266
Mumbai: (+91) 22 2579 7589
Hyderabad: (+91) 40 4015 5466

Ireland
SIGMA-ALDRICH IRELAND LTD.
Free Tel: 1800 200 888
Free Fax: 1800 600 222
Tel: (+353) 1 404 1900
Fax: (+353) 1 404 1910

Israel
SIGMA-ALDRICH ISRAEL LTD.
Free Tel: 1 800 70 2222
Tel: (+972) 8 948 4100
Fax: (+972) 8 948 4200

Italy
SIGMA-ALDRICH S.r.l.
Numero Verde: 800 827018
Tel: (+39) 02 3341 7310
Fax: (+39) 02 3801 0737

Japan
SIGMA-ALDRICH JAPAN K.K.
Tel: (+81) 3 5796 7300
Fax: (+81) 3 5796 7315

Korea
SIGMA-ALDRICH KOREA
Free Tel: (+82) 80 023 7111
Free Fax: (+82) 80 023 8111
Tel: (+82) 31 329 9000
Fax: (+82) 31 329 9090

Malaysia
SIGMA-ALDRICH (M) SDN. BHD
Tel: (+60) 3 5635 3321
Fax: (+60) 3 5635 4116

Mexico
SIGMA-ALDRICH QUÍMICA, S.A. de C.V.
Free Tel: 01 800 007 5300
Free Fax: 01 800 712 9920
Tel: 52 722 276 1600
Fax: 52 722 276 1601

The Netherlands
SIGMA-ALDRICH CHEMIE BV
Free Tel: 0800 022 9088
Free Fax: 0800 022 9089
Tel: (+31) 78 620 5411
Fax: (+31) 78 620 5421

New Zealand
SIGMA-ALDRICH NEW ZEALAND LTD.
Free Tel: 0800 936 666
Free Fax: 0800 937 777
Tel: (+61) 2 9841 0555
Fax: (+61) 2 9841 0500

Norway
SIGMA-ALDRICH NORWAY AS
Tel: (+47) 23 17 60 60
Fax: (+47) 23 17 60 50

Poland
SIGMA-ALDRICH Sp. z o.o.
Tel: (+48) 61 829 01 00
Fax: (+48) 61 829 01 20

Portugal
SIGMA-ALDRICH QUÍMICA, S.A.
Free Tel: 800 202 180
Free Fax: 800 202 178
Tel: (+351) 21 924 2555
Fax: (+351) 21 924 2610

Russia
SIGMA-ALDRICH RUS, LLC
Tel: +7 (495) 621 6037
+7 (495) 621 5828
Fax: +7 (495) 621 5923

Singapore
SIGMA-ALDRICH PTE. LTD.
Tel: (+65) 6779 1200
Fax: (+65) 6779 1822

South Africa
SIGMA-ALDRICH
SOUTH AFRICA (PTY) LTD.
Free Tel: 0800 1100 75
Free Fax: 0800 1100 79
Tel: (+27) 11 979 1188
Fax: (+27) 11 979 1119

Spain
SIGMA-ALDRICH QUÍMICA, S.A.
Free Tel: 900 101 376
Free Fax: 900 102 028
Tel: (+34) 91 661 99 77
Fax: (+34) 91 661 96 42

Sweden
SIGMA-ALDRICH SWEDEN AB
Tel: (+46) 8 742 4200
Fax: (+46) 8 742 4243

Switzerland
SIGMA-ALDRICH CHEMIE GmbH
Free Tel: 0800 80 00 80
Free Fax: 0800 80 00 81
Tel: (+41) 81 755 2828
Fax: (+41) 81 755 2815

United Kingdom
SIGMA-ALDRICH COMPANY LTD.
Free Tel: 0800 717 181
Free Fax: 0800 378 785
Tel: (+44) 1747 833 000
Fax: (+44) 1747 833 313
SAFC (UK) Free Tel: 01202 712305

United States
SIGMA-ALDRICH
P.O. Box 14508
St. Louis, Missouri 63178
Toll-Free: 800 325 3010
Toll-Free Fax: 800 325 5052
Call Collect: (+1) 314 771 5750
Tel: (+1) 314 771 5765
Fax: (+1) 314 771 5757

Internet
sigma-aldrich.com

Green U Power

© Mixed Sources
Product group from well-managed forests, controlled sources and recycled wood or fiber
www.fsc.org Cert no. SGS-COC-003338
© 1996 Forest Stewardship Council
FSC
10%

World Headquarters
3050 Spruce St., St. Louis, MO 63103
(314) 771-5765
sigma-aldrich.com

Order/Customer Service (800) 325-3010 • Fax (800) 325-5052
Technical Service (800) 325-5832 • sigma-aldrich.com/techservice
Development/Bulk Manufacturing Inquiries SAFC™ (800) 244-1173

*Accelerating Customers' Success through Leadership in **Life Science, High Technology** and **Service***

©2008 Sigma-Aldrich Co. All rights reserved. SIGMA, ®, SAFC, SAFC™, SIGMA-ALDRICH, ALDRICH, ®, FLUKA, ®, and SUPELCO, ® are trademarks belonging to Sigma-Aldrich Co. and its affiliate Sigma-Aldrich Biotechnology, L.P. Sigma brand products are sold through Sigma-Aldrich, Inc. Sigma-Aldrich, Inc. warrants that its products conform to the information contained in this and other Sigma-Aldrich publications. Purchaser must determine the suitability of the product(s) for their particular use. Additional terms and conditions may apply. Please see reverse side of the invoice or packing slip.

KGQ
03904-503403
0028

SIGMA-ALDRICH™

Sigma-Aldrich
3050 Spruce Street
St. Louis, MO 63103 USA
sigma-aldrich.com